LA-UR- 02-5229

Approved for public release; distribution is unlimited.

Title: FREQUENCY-SHIFT ESTIMATE FOR AN SNS SUPERCONDUCTING RF CAVITY

Author(s): Sung-il Kwon, SNS-02

Submitted to:

Los Alamos
NATIONAL LABORATORY

FREQUENCY-SHIFT ESTIMATE FOR AN SNS SUPERCONDUCTING RF CAVITY

Sung-il Kwon[1] and Amy Regan

SNS-2, RF Technology Group

SNS Division, Los Alamos National Laboratory

1 Corresponding author: SNS-2, RF Power Group, SNS Division, Los Alamos National Laboratory, Mail Stop H827, P.O. Box 1663, Los Alamos, NM 87544, USA, email: skwon@lanl.gov, fax: 665-2818

1. INTRODUCTION

The superconducting RF (SRF) cavities that are to be used for the SNS project must have their resonance frequencies tuned to within a few Hertz of the 805-MHz operating frequency. The resonance frequencies of cavities alter due to such factors as ambient temperature change, helium pressure variation, Lorentz-force detuning, and microphonics. This report addresses cavity-tune algorithms. The cavity-tune algorithms will be implemented using the Texas Instruments (TI) digital-signal processor (DSP) TMS320C6203B and the Experimental Physics and Industrial Control System (EPICS) interfaces. Computation of the tuning frequency will be achieved by the TMS320C6203B DSP and by a direct digital synthesis (DDS) technique using the AD9852 DDS by Analog Devices.

2. SRF CAVITY MODEL AND FREQUENCY-SHIFT MODEL

An SRF cavity is given by the following state-space model:

$$\dot{z} = A_z(\Delta\omega)z + B_z u + B_{zI} I \tag{2.1}$$

$$y = C_z z, \tag{2.2}$$

where

$$A_z(\Delta\omega) = \begin{bmatrix} -\frac{1}{\tau_L} & -\Delta\omega \\ \Delta\omega & -\frac{1}{\tau_L} \end{bmatrix}$$

$$B_z = \begin{bmatrix} \frac{2}{Z_o}c_1 & -\frac{2}{Z_o}c_3 \\ \frac{2}{Z_o}c_3 & \frac{2}{Z_o}c_1 \end{bmatrix}, \qquad B_{zI} = \begin{bmatrix} -2c_1\zeta & 2c_3\zeta \\ -2c_3\zeta & -2c_1\zeta \end{bmatrix}, \tag{2.3}$$

$$C_z = \begin{bmatrix} 1 & 0 \\ 0 & 1 \end{bmatrix},$$

$$z = \begin{bmatrix} z_1 \\ z_2 \end{bmatrix} = \begin{bmatrix} V_I \\ V_Q \end{bmatrix}, \quad u = \begin{bmatrix} u_1 \\ u_2 \end{bmatrix} = \begin{bmatrix} HPRF_I \\ HPRF_Q \end{bmatrix}, \quad I = \begin{bmatrix} I_I \\ I_Q \end{bmatrix},$$

and

$$\Delta\omega = \Delta\omega_B + \Delta\omega_L + \Delta\omega_{MCP}, \tag{2.4}$$

$$c_1 = \frac{R_{cu}}{\tau}, \quad c_3 = \frac{R_{cu}}{2Q_o\tau},$$

with the following definitions of variables and parameters:

$\Delta\omega_B$ = pre-detuning frequency shift against beam loading [rad/s],

$\Delta\omega_L$ = frequency shift caused by Lorentz-force detuning [rad/s],

$\Delta\omega_{MCP}$ = frequency shift due to Microphonics [rad/s],

$\tau = \frac{2Q_o}{\omega_o}$ = unloaded cavity-damping time constant [s],

$\tau_L = \frac{2Q_L}{\omega_o}$ = loaded cavity-damping time constant [s],

ϕ_s = synchronous phase,

Q_o = cavity resonator unloaded quality factor,

ω_o = cavity resonance frequency [rad/s],

R_{cu} = resistance of the equivalent circuit of the cavity transformed to RF generator [Ω],

R_o = transmission line characteristic impedance [Ω],

ζ = transformation ratio,

V_{fI}, V_{fQ} = forward I/Q voltage [V],

I_I, I_Q = beam current in I/Q [A], and

V_I, V_Q = cavity Field in I/Q [V].

Note that in the above model, $\Delta\omega$ is the sum of the pre-detuning, $\Delta\omega_B$; the Lorentz-force detuning, $\Delta\omega_L$; and microphonics, $\Delta\omega_{MCP}$. The state-space model given by (2.1)-(2.2) can be written as

$$\dot{z} = A_z z + B_z u + B_{zI} I + \begin{bmatrix} -\Delta\omega y_2 \\ \Delta\omega y_1 \end{bmatrix} \tag{2.5}$$

$$y = C_z z , \tag{2.6}$$

where

$$A_z = \begin{bmatrix} -\frac{1}{\tau_L} & 0 \\ 0 & -\frac{1}{\tau_L} \end{bmatrix}. \tag{2.7}$$

The objective of this report is to design an observer such that the estimate $\Delta\hat{\omega}$ yielded by the observer exponentially approaches the frequency shift $\Delta\omega$. As mentioned in the previous section, when the Lorentz-force detuning model includes all mechanical mode dynamics, the observer structure may be complicated, which increases computational complexity. Instead of this complex higher-order model, the frequency shift is modeled as

$$\Delta\dot{\omega} = 0 . \tag{2.8}$$

This model (2.8) is widely used for disturbance that is constant or which varies slowly. The augmented state-space model, with outputs y_1, y_2 and inputs u_1, u_2 is

$$\begin{bmatrix} \dot{z}_1 \\ \dot{z}_2 \\ \Delta\dot{\omega} \end{bmatrix} = \begin{bmatrix} 0 & 0 & -y_2 \\ 0 & 0 & y_1 \\ 0 & 0 & 0 \end{bmatrix} \begin{bmatrix} z_1 \\ z_2 \\ \Delta\omega \end{bmatrix} + \begin{bmatrix} -\frac{1}{\tau_L} & 0 \\ 0 & -\frac{1}{\tau_L} \\ 0 & 0 \end{bmatrix} \begin{bmatrix} y_1 \\ y_2 \end{bmatrix} + \begin{bmatrix} \frac{2}{Z_o}c_1 & -\frac{2}{Z_o}c_3 \\ \frac{2}{Z_o}c_3 & \frac{2}{Z_o}c_1 \\ 0 & 0 \end{bmatrix} \begin{bmatrix} u_1 \\ u_2 \end{bmatrix} + \begin{bmatrix} B_{zI} \\ 0 \end{bmatrix} I \tag{2.9}$$

$$y = \begin{bmatrix} C_z & 0 \end{bmatrix} \begin{bmatrix} z_1 \\ z_2 \\ \omega \end{bmatrix}. \tag{2.10}$$

3. NONLINEAR FIRST-ORDER DYNAMIC OBSERVER

Consider the state equation for the cavity field quadrature (Q).

$$\dot{z}_2 = y_1\Delta\omega - \frac{1}{\tau_L}z_2 + \frac{2}{Z_o}c_3u_1 + \frac{2}{Z_o}c_1u_2 - 2c_3\mathcal{G}I_I - 2c_1\mathcal{G}I_Q . \tag{3.1}$$

The equation (3.1) is written as

$$y_1\Delta\omega = \dot{z}_2 + \frac{1}{\tau_L}z_2 - \frac{2}{Z_o}c_3u_1 - \frac{2}{Z_o}c_1u_2 + 2c_3\mathcal{G}I_I + 2c_1\mathcal{G}I_Q . \tag{3.2}$$

Consider the term $2c_3\mathcal{G}I_I + 2c_1\mathcal{G}I_Q$ on the right-hand side of (3.2). It follows that

$$\begin{aligned}
2c_3\mathcal{G}I_I + 2c_1\mathcal{G}I_Q &= 2\frac{R_{cu}}{2\pi Q_o}\frac{Vc}{V_f}I_b\cos(\phi_s) + 2\frac{R_{cu}}{\tau}\frac{Vc}{V_f}I_b\sin(\phi_s) \\
&= 2\frac{\omega_o}{2Q_o}\frac{1}{2Q_o}\frac{V_f^2}{2P_{cu}}\frac{Vc}{V_f}I_b\cos(\phi_s) + 2\frac{\omega_o}{2Q_o}\frac{V_f^2}{2P_{cu}}\frac{Vc}{V_f}I_b\sin(\phi_s) \\
&= \frac{\omega_o}{2Q_o}\frac{1}{2Q_o}\frac{Vc}{P_{cu}}I_b\cos(\phi_s)V_f + \frac{\omega_o}{2Q_o}\frac{Vc}{P_{cu}}I_b\sin(\phi_s)V_f \\
&= \frac{\omega_o}{2Q_o}\frac{1}{2Q_o}\frac{P_b}{P_{cu}}V_f + \frac{\omega_o}{2Q_o}\frac{P_b}{P_{cu}}\tan(\phi_s)V_f \\
&= \frac{\omega_o}{2Q_o}\frac{P_b}{P_{cu}}\left(\frac{1}{2Q_o} + \tan(\phi_s)\right)V_f ,
\end{aligned} \tag{3.3}$$

where V_f is the desired cavity field amplitude, P_{cu} is the wall power dissipation, P_b is the beam power, V_c is the design cavity voltage, and ϕ_s is the synchronous phase. Since $Q_o >> 1$ and $\frac{P_b}{P_{cu}} \approx \beta$ for an SRF cavity, equation (3.3) reduces to

$$2c_3\mathcal{G}I_I + 2c_1\mathcal{G}I_Q = \frac{\omega_o}{2Q_L}\tan(\phi_s)V_f . \tag{3.4}$$

Consider the pre-detuning frequency $\Delta\omega_B$. Since

$$\tan(\psi) = 2Q_L\frac{\Delta\omega_B}{\omega_o} , \tag{3.5}$$

where ψ is the detuning angle due to the beam loading. Because the beam-loading factor $\beta >> 1$ for an SRF cavity, $\tan(\psi)$, is given by

$$\tan(\psi) = \frac{\beta - 1}{\beta + 1}\tan(\phi_s) \approx \tan(\phi_s) , \tag{3.6}$$

it follows from (3.5) and (3.6) that

$$y_1\Delta\omega_B = y_1\frac{\omega_o}{2Q_L}\tan(\phi_s). \tag{3.7}$$

Now consider (3.4) and (3.7). When the cavity operates on resonance with a generator and the cavity field is settled down to the neighborhood of the desired values, then the imaginary part of the cavity field, y_2, is close to zero, which yields $V_f \approx \sqrt{y_1^2 + y_2^2} \approx y_1$. Therefore,

$$y_1 \Delta\omega_B \approx 2c_3 \varsigma I_I + 2c_1 \varsigma I_Q$$

and (3.2) can be written as

$$y_1 \Delta\omega = \dot{z}_2 + \frac{1}{\tau_L} z_2 - \frac{2}{Z_o} c_3 u_1 - \frac{2}{Z_o} c_1 u_2 , \tag{3.8}$$

where $\Delta\omega = \Delta\omega_L + \Delta\omega_{MCP}$.

In summary, it follows from (2.4) and (3.8) that (3.2) has two forms depending on whether or not the cavity is loaded with beam. When beam is not loaded, (3.2) reduces to

$$y_1 \Delta\omega = \dot{z}_2 + \frac{1}{\tau_L} z_2 - \frac{2}{Z_o} c_3 u_1 - \frac{2}{Z_o} c_1 u_2$$

$$\Delta\omega = \Delta\omega_B + \Delta\omega_L + \Delta\omega_{MCP} . \tag{3.9}$$

When beam is loaded, (3.2) reduces to

$$y_1 \Delta\omega = \dot{z}_2 + \frac{1}{\tau_L} z_2 - \frac{2}{Z_o} c_3 u_1 - \frac{2}{Z_o} c_1 u_2$$

$$\Delta\omega = \Delta\omega_L + \Delta\omega_{MCP} . \tag{3.10}$$

For the frequency-shift estimation, a disturbance observer is proposed as follows:

$$\Delta\dot{\hat{\omega}} = -L y_1 \Delta\hat{\omega} + L\left(\dot{z}_2 + \frac{1}{\tau_L} z_2 - \frac{2}{Z_o} c_3 u_1 - \frac{2}{Z_o} c_1 u_2 \right). \tag{3.11}$$

It follows from (2.8) and (3.11) that the observer-error dynamics are given by

$$\dot{e} = \Delta\dot{\omega} - \Delta\dot{\hat{\omega}} = L y_1 \Delta\hat{\omega} - L\left(\dot{z}_2 + \frac{1}{\tau_L} z_2 - \frac{2}{Z_o} c_3 u_1 - \frac{2}{Z_o} c_1 u_2 \right)$$

$$= L y_1 \Delta\hat{\omega} - L y_1 \Delta\omega$$

$$= -L y_1 e . \tag{3.12}$$

The observer gain, L, is determined so that the characteristic equation

$$s + L y_1 = 0 \tag{3.13}$$

has a desired root in the left-half plane of the complex domain. The observer-error dynamics (3.12) show that for a properly chosen gain, L, the estimate, $\hat{\omega}$, asymptotically converges to $\Delta\omega_B + \Delta\omega_L + \Delta\omega_{MCP}$ when beam is not loaded, and to $\Delta\omega_L + \Delta\omega_{MCP}$ when beam is loaded.

The observer (3.11) is difficult to implement in practical terms because the derivative term $\dot{z}_2$ is noisy and is hard to measure. Instead, the following new variable is introduced:

$$\hat{g}_L = \Delta\hat{\omega} - p(z_2) , \tag{3.14}$$

where $p(z_2)$ is a nonlinear function of z_2, to be determined as follows:

The derivative of (3.14) with respect to time is

$$\begin{aligned}\dot{\hat{g}}_L &= \Delta\dot{\hat{\omega}} - \frac{\partial p(z_2)}{\partial z_2}\frac{dz_2}{dt} \\ &= -Ly_1\Delta\hat{\omega} + L\left(\dot{z}_2 + \frac{1}{\tau_L}z_2 - \frac{2}{Z_o}c_3u_1 - \frac{2}{Z_o}c_1u_2\right) - \frac{\partial p(z_2)}{\partial z_2}\dot{z}_2 \\ &= -Ly_1\hat{g}_L + L\left(\dot{z}_2 + \frac{1}{\tau_L}z_2 - \frac{2}{Z_o}c_3u_1 - \frac{2}{Z_o}c_1u_2 - y_1p(z_2)\right) - \frac{\partial p(z_2)}{\partial z_2}\dot{z}_2 .\end{aligned} \tag{3.15}$$

When $p(z_2)$ is determined so that it satisfies

$$\frac{\partial p(z_2)}{\partial z_2} = L , \tag{3.16}$$

then (3.15) reduces to

$$\dot{\hat{g}}_L = -Ly_1\hat{g}_L + L\left(\frac{1}{\tau_L}z_2 - \frac{2}{Z_o}c_3u_1 - \frac{2}{Z_o}c_1u_2 - y_1p(z_2)\right), \tag{3.17}$$

and the Lorentz-force detuning estimate is given by

$$\Delta\hat{\omega} = \hat{g}_L + p(z_2) . \tag{3.18}$$

It is easily verified that the observer-error dynamics are given by

$$\dot{e} = \Delta\dot{\omega} - \Delta\dot{\hat{\omega}} = -\dot{\hat{g}}_L - \frac{\partial p(z_2)}{\partial z_2}\frac{dz_2}{dt} = -Ly_1e . \tag{3.19}$$

The estimate $\Delta\hat{\omega}$ approaches the frequency shift $\Delta\omega$ if L is chosen such that (3.19) is asymptotically stable. One possible solution for L is

$$L = \frac{l}{y_1}, \tag{3.20}$$

where l is a positive constant. In this case, the observer-error dynamics become

$$\dot{e} + le = 0 , \tag{3.21}$$

and the convergence rate can be specified by the parameter l. From (3.16), the corresponding $p(z_2)$ becomes

$$p(z_2) = \frac{l}{y_1}z_2 . \tag{3.22}$$

The constant, c_3, is very small, such that by plugging (3.20) and (3.22) into (3.17) and (3.18), (3.17) and (3.18) are reduced to

$$\dot{\hat{g}}_L = -l\hat{g}_L + l\left(\left(\frac{1}{\tau_L} - l\right)\frac{z_2}{y_1} - \frac{2}{Z_o}c_1\frac{u_2}{y_1}\right) \tag{3.23}$$

$$\Delta\hat{\omega} = \hat{g}_L + l\frac{z_2}{y_1} . \tag{3.24}$$

The discrete-time version of the frequency-shift observer is obtained from (3.23) and (3.24). Let t_s be the sampling frequency. The discrete-time frequency-shift observer is

$$\hat{g}_L(k+1) = (1 - t_s l)\hat{g}_L(k) + t_s l\left(\left(\frac{1}{\tau_L} - l\right)\frac{z_2(k)}{y_1(k)} - \frac{2}{Z_o}c_1\frac{u_2(k)}{y_1(k)}\right) \tag{3.25}$$

$$\Delta\hat{\omega}(k) = \hat{g}_L(k) + l\frac{z_2(k)}{y_1(k)}. \tag{3.26}$$

Because (3.25) is a first-order differential equation, the following relationship is required to make the observer stable:

$$-1 \le 1 - t_s l \le 1.$$

That is,

$$l \le \frac{2}{t_s}. \tag{3.27}$$

For example, for the 200-kHz sampling frequency, the gain, l, should be

$$l \le 4\times 10^5.$$

Let

$$k_1 = 1 - t_s l, \tag{3.28}$$

$$k_2 = t_s l\left(\frac{1}{\tau_L} - l\right), \text{ and} \tag{3.29}$$

$$k_3 = -t_s l\frac{2}{Z_o}c_1, \tag{3.30}$$

then (3.25) becomes

$$\hat{g}_L(k+1) = k_1\hat{g}_L(k) + k_2\frac{z_2(k)}{y_1(k)} + k_3\frac{u_2(k)}{y_1(k)}. \tag{3.31}$$

Discrete-Time Frequency-Shift Observer:

$$\boxed{\begin{aligned}\hat{g}_L(k+1) &= k_1\hat{g}_L(k) + k_2\frac{z_2(k)}{y_1(k)} + k_3\frac{u_2(k)}{y_1(k)}\\ \Delta\hat{\omega}(k) &= \hat{g}_L(k) + l\frac{z_2(k)}{y_1(k)}\end{aligned}} \tag{3.32}$$

Note that when the input is zero, as is the case when the nonzero driving RF becomes zero (RF OFF period), then the frequency-shift observer becomes

$$\hat{g}_L(k+1) = k_1 \hat{g}_L(k) + k_2 \frac{z_2(k)}{y_1(k)}$$
$$\Delta\hat{\omega}(k) = \hat{g}_L(k) + l \frac{z_2(k)}{y_1(k)} \tag{3.33}$$

In the steady state where

$$\hat{g}_{LSS} = \hat{g}_L(k+1) = \hat{g}_L(k),$$

the frequency shift observer is represented by

$$\hat{g}_{LSS} = \frac{k_2}{1-k_1}\frac{z_2(k)}{y_1(k)} + \frac{k_3}{1-k_1}\frac{u_2(k)}{y_1(k)}$$
$$\Delta\hat{\omega}(k) = \hat{g}_L(k) + l \frac{z_2(k)}{y_1(k)} \tag{3.34}$$

Example 1. Consider an SRF cavity that has an operating frequency of 805 MHz and a loaded Q factor of $Q_L = 7.3\times10^5$. Assume that the transmission line impedance is 50Ω. The time constant, τ_L, is $\tau_L = \frac{2Q_L}{2\pi\cdot 805\times10^5} = 2.8865e-4$ and $\frac{2}{Z_o}c_1 = 6919.9$. Assume that the sampling frequency is 200 kHz. Let the gain, l, be 1×10^5. Then, $k_1 = 0.5$, $k_2 = 48267.8$, and $k_3 = -3459.9$.

4. NONLINEAR ALGEBRAIC OBSERVER

Consider the following SRF cavity model, (2.1)-(2.4), without beam loading:

$$\dot{z}_1 = -\frac{1}{\tau_L} z_1 - \Delta\omega z_2 + \frac{2}{Z_o} c_1 u_1 - \frac{2}{Z_o} c_3 u_2 \tag{4.1}$$

$$\dot{z}_2 = \Delta\omega z_1 - \frac{1}{\tau_L} z_2 + \frac{2}{Z_o} c_3 u_1 + \frac{2}{Z_o} c_1 u_2. \tag{4.2}$$

Multiplying both sides of (4.1) with z_2, we obtain

$$z_2 \dot{z}_1 = -\frac{1}{\tau_L} z_1 z_2 - \Delta\omega z_2^2 + \frac{2}{Z_o} c_1 u_1 z_2 - \frac{2}{Z_o} c_3 u_2 z_2. \tag{4.3}$$

Multiplying both sides of (4.2) with z_1, we obtain

$$z_1 \dot{z}_2 = \Delta\omega z_1^2 - \frac{1}{\tau_L} z_1 z_2 + \frac{2}{Z_o} c_3 u_1 z_1 + \frac{2}{Z_o} c_1 u_2 z_1. \tag{4.4}$$

Subtracting both sides of (4.4) from (4.3), we obtain

$$z_2 \dot{z}_1 - z_1 \dot{z}_2 = -\Delta\omega (z_1^2 + z_2^2) + \frac{2}{Z_o} c_1 u_1 z_2 - \frac{2}{Z_o} c_3 u_2 z_2 - \frac{2}{Z_o} c_3 u_1 z_1 - \frac{2}{Z_o} c_1 u_2 z_1. \tag{4.5}$$

Note that, for an SRF cavity, due to the large unloaded Q, $c_3 \approx 0$. Then, (4.5) is approximated to

$$z_2 \dot{z}_1 - z_1 \dot{z}_2 = -\Delta\omega (z_1^2 + z_2^2) + \frac{2}{Z_o} c_1 u_1 z_2 - \frac{2}{Z_o} c_1 u_2 z_1. \tag{4.6}$$

Hence, the frequency shift is calculated as

$$\Delta\omega = -\frac{(z_2 \dot{z}_1 - z_1 \dot{z}_2)}{z_1^2 + z_2^2} + \frac{2}{Z_o} c_1 \frac{u_1 z_2 - u_2 z_1}{z_1^2 + z_2^2}. \tag{4.7}$$

The first term of the right-hand side of (4.7) is the transient dynamics. Hence, in steady state, (4.7) is reduced to

$$\Delta\omega = \frac{2}{Z_o} c_1 \frac{u_1 z_2 - u_2 z_1}{z_1^2 + z_2^2}. \tag{4.8}$$

In the discrete-time system, the frequency shift is calculated from the discrete-time representation of (4.6).

$$z_2(k)\frac{z_1(k+1) - z_1(k)}{t_s} - z_1(k)\frac{z_2(k+1) - z_2(k)}{t_s}$$

$$= -\Delta\omega(k)(z_1^2(k) + z_2^2(k)) + \frac{2}{Z_o} c_1 u_1(k) z_2(k) - \frac{2}{Z_o} c_1 u_2(k) z_1(k), \tag{4.9}$$

where t_s is the sampling time and k is the sample number.

Hence,

$$\Delta\omega(k) = \frac{1}{t_s} \frac{z_2(k) z_1(k+1) - z_1(k) z_2(k+1)}{z_1^2(k) + z_2^2(k)} + \frac{2}{Z_o} c_1 \frac{u_1(k) z_2(k) - u_2(k) z_1(k)}{z_1^2(k) + z_2^2(k)}. \tag{4.10}$$

The frequency shift given by (4.10) has the predictive terms $z_1(k+1)$ and $z_2(k+1)$. However, when the frequency-shift calculation is a batch process as it is when we implement it in our DSP software and hardware electronics, the predictive terms do not yield computational difficulty. In steady state, since $z_1(k+1)=z_1(k)$, $z_2(k+1)=z_2(k)$, (4.10) is reduced to

$$\Delta\omega(k)=\frac{2}{Z_o}c_1\frac{u_1(k)z_2(k)-u_2(k)z_1(k)}{z_1^2(k)+z_2^2(k)}. \tag{4.11}$$

Nonlinear Algebraic Observer:

$$\boxed{\Delta\omega(k)=\frac{2}{Z_o}c_1\frac{u_1(k)z_2(k)-u_2(k)z_1(k)}{z_1^2(k)+z_2^2(k)}} \tag{4.12}$$

Now consider long-term resonance control, that is, RF-pulse-based resonance control. A single-frequency estimate value for each RF pulse must be obtained because the RF driving frequency is updated once for each RF pulse, even though the frequency shift is estimated by (4.10) or (4.12) for one RF pulse period. We can use the last sample of an RF pulse, or we can take the average of N samples of frequency-shift estimates. Usually, the second method is recommended. Another problem is that (4.10) or (4.12) is dependent upon the cavity parameters, Z_o, c_1. Of course, we can obtain these parameters with the open-loop system parameter-estimation algorithm. Or, we can discard dependence of (4.10) or (4.12) on the cavity parameters by introducing the lumped controller gain, which will be shown in the following.

Let n be the RF pulse number and let $\Delta\overline{\omega}(n)$ be the average of N samples of nth RF pulse. Note that in order to discard the transients during one RF pulse, a starting point of averaging, N_0, is specified.

$$\Delta\overline{\omega}(n)=\frac{1}{N}\sum_{k=N_0}^{N_0+N-1}\frac{u_1(k)z_2(k)-u_2(k)z_1(k)}{z_1^2(k)+z_2^2(k)}, \tag{4.13}$$

which is not dependent upon the cavity parameters, Z_o, c_1.

To obtain the asymptotic convergence of $\Delta\overline{\omega}(n)$ to zero as the RF pulse number increases, the update of the driving RF frequency is given by the following difference equations:

$$\Delta f(n+1)=\Delta f(n)+K\Delta\overline{\omega}(n) \tag{4.14}$$

$$f(n+1)=f(n)+\Delta f(n+1), \tag{4.15}$$

where K is a gain. At the nth step, (4.13)-(4.14) can be written as

$$\Delta f(n) = \Delta f(0) + K\sum_{i=0}^{n-1} \Delta\overline{\omega}(i) \tag{4.16}$$

$$f(n) = f(0) + n\Delta f(0) + K\sum_{i=0}^{n-1} (n-i)\Delta\overline{\omega}(i). \tag{4.17}$$

Theoretically, the convergence rate of the above algorithm is dependent upon K. When K is chosen properly, $\Delta\overline{\omega}(n)$ converges to zero within a few steps. However, when K is too small, the convergence is very slow. To improve the convergence rate, the following adaptive rule is proposed:

$$K(n+1) = K(n) + \varepsilon \frac{1}{T_{RF}} \left\| \Delta\overline{\omega}(n) \right\|, \tag{4.18}$$

where ε is a small positive constant and T_{RF} is the period of RF pulse. Then, the driving frequency update equations are reduced to

$$\Delta\overline{\omega}(n) = \frac{1}{N} \sum_{k=N_0}^{N_0+N-1} \frac{2}{Z_o} c_1 \frac{u_1(k)z_2(k) - u_2(k)z_1(k)}{z_1^2(k) + z_2^2(k)} \tag{4.19}$$

$$K(n+1) = K(n) + \varepsilon \frac{1}{T_{RF}} \left\| \Delta\overline{\omega}(n) \right\| \tag{4.20}$$

$$\Delta f(n+1) = \Delta f(n) + K(n)\Delta\overline{\omega}(n) \tag{4.21}$$

$$f(n+1) = f(n) + \Delta f(n+1). \tag{4.22}$$

5. SWEEP-MODE RESONANCE CONTROL

The idea of the sweep-mode resonance control of an SRF cavity is based on the information in Figure 5.1. In Figure 5.1, a resonator's magnitude and phase are plotted with respect to frequency. At resonance, the magnitude is at its peak and the phase changes its sign. Note that the phase plot has the same characteristics as the inverse tangent curve. Also, the equation (4.11) shows that the frequency shift is inversely proportional to the square of the cavity field amplitude.

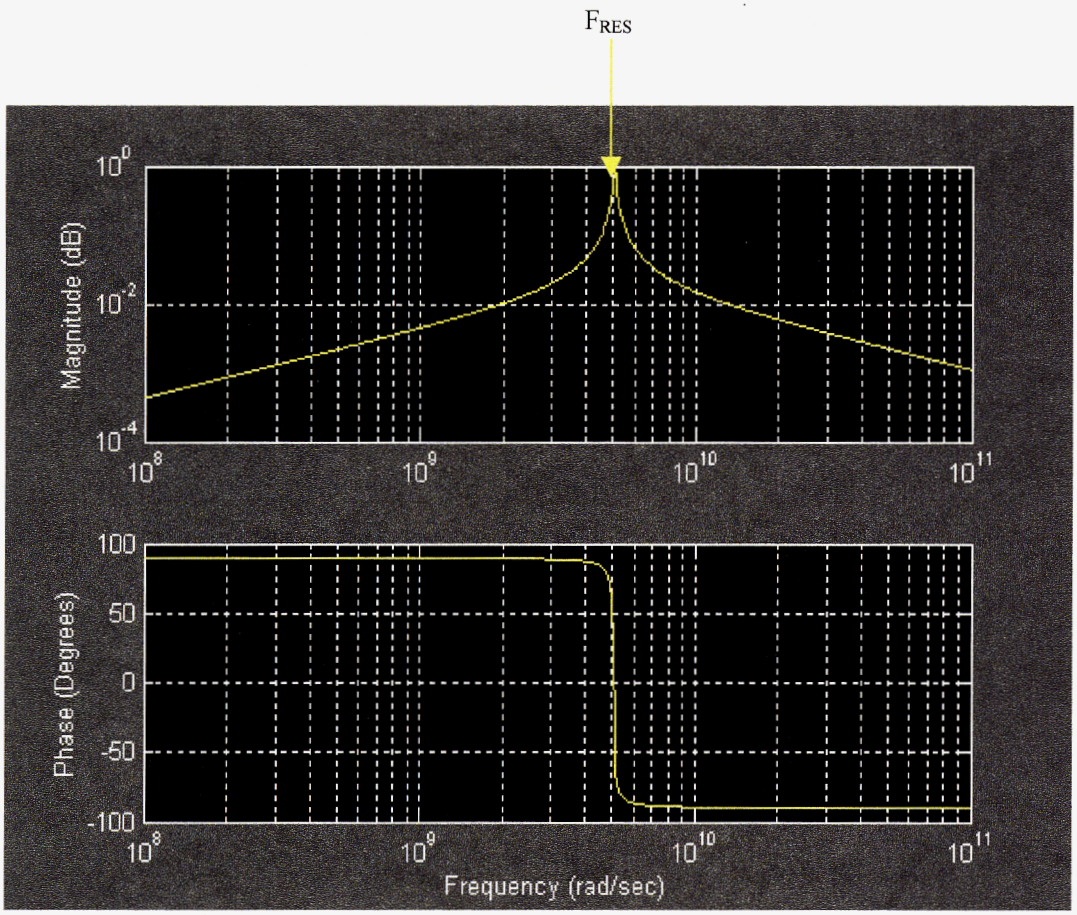

Figure 5.1. Cavity Frequency Response Around the Resonance Frequency. The cavity resonance frequency is 805 MHz.

When the RF drive frequency is tuned to $F_0 + \Delta f(n)$ at the nth RF pulse, the modulated output at the (n+1)th RF pulse is

$$V_{MOD}(k) = I_L(k)\cos\left(2\pi(F_0 + \Delta f(n))k\right) + Q_L(k)\sin\left(2\pi(F_0 + \Delta f(n))k\right), \quad (5.1)$$

where $I_L(k)$ and $Q_L(k)$ are input in-phase (I) and Q at the kth sample.

This signal is amplified by a high-power amplifier, such as a klystron, and passes through the SRF cavity whose resonance frequency is $F_0 + \Delta f(n)$. When the amplification gain at the high-power amplifier is assumed to be 1, and it is assumed that there is no loss in the transmission line and the cavity, the demodulated signals (with the frequency F_0) of the SRF cavity output are given by

$$I_{DEMOD0}(k) = 2V_{MOD}\cos(2\pi F_0 k) = 2\big(I_L(k)\cos(2\pi(F_0 + \Delta f(n))k) + Q_L(k)\sin(2\pi(F_0 + \Delta f(n))k)\big)\cos(2\pi F_0 k)$$
$$= I_L(k)\big(\cos(2\pi(2F_0 + \Delta f(n))k) + \cos(2\pi\Delta f(n)k)\big) + Q_L(k)\big(\sin(2\pi(2F_0 + \Delta f(n))k) + \sin(2\pi\Delta f(n)k)\big) \quad (5.2)$$

and

$$Q_{DEMOD0}(k) = 2V_{MOD}\sin(2\pi F_0 k) = 2\big(I_L(k)\cos(2\pi(F_0 + \Delta f(n))k) + Q_L(k)\sin(2\pi(F_0 + \Delta f(n))k)\big)\sin(2\pi F_0 k)$$
$$= I_L(k)\big(\sin(2\pi(2F_0 + \Delta f(n))k) - \sin(2\pi\Delta f(n)k)\big) + Q_L(k)\big(-\cos(2\pi(2F_0 + \Delta f(n))k) + \cos(2\pi\Delta f(n)k)\big), \quad (5.3)$$

where k is a sample number. The signals (5.2) and (5.3) are filtered, and the final demodulated I and Q signals are obtained.

$$z_1(k) = I_{DEMOD}(k) = I_L(k)\cos(2\pi\Delta f(n)k) + Q_L(k)\sin(2\pi\Delta f(n)k) \quad (5.4)$$

and

$$z_2(k) = Q_{DEMOD}(k) = -I_L(k)\sin(2\pi\Delta f(n)k) + Q_L(k)\cos(2\pi\Delta f(n)k) \quad (5.5)$$

(5.4) and (5.5) can be written by

$$\begin{bmatrix} z_1(k) \\ z_2(k) \end{bmatrix} = \begin{bmatrix} I_{DEMOD}(k) \\ Q_{DEMOD}(k) \end{bmatrix} = \begin{bmatrix} \cos(2\pi\Delta f(n)k) & \sin(2\pi\Delta f(n)k) \\ -\sin(2\pi\Delta f(n)k) & \cos(2\pi\Delta f(n)k) \end{bmatrix} \begin{bmatrix} I_L(k) \\ Q_L(k) \end{bmatrix}. \quad (5.6)$$

It can be easily verified that the amplitude of the demodulated signals is the same as that of the input I and Q.

$$(z_1(k)) + (z_2(k))^2 = (I_{DEMOD}(k)) + (Q_{DEMOD}(k))^2 = (I_L(k))^2 + (Q_L(k))^2. \quad (5.7)$$

However, the phase is $2\pi\Delta f(n)k$, which varies during an RF pulse. For instance, the total samples during an RF pulse of 1.3 msec duration is $N_s = 1.3e-3 \cdot 20e6 = 26000$, where the sampling frequency is 20 MHz. Hence, the phase rotation number is $\Delta f(n) \cdot 1.3e-3$, and when $\Delta f(n)$ is 20 kHz, the phase rotation is 26. This means that during one RF pulse, the phasor rotates a circle of radius one 26 times. As a consequence, the phase-related information on the direct change of the frequency sweep is not appropriate when $\Delta f(n)$ is large.

Instead, the information related to the magnitude response, as shown in Figure 5.1, is dealt with differently. The direction of the frequency sweep is changed when the derivative (in continuous-time domain)/the difference (in discrete-time domain) of the magnitude (and hence the square of the magnitude), with respect to frequency, changes its sign, as illustrated in Figure 5.2. Because it is difficult to implement the square-root hardware and to implement the square root in the fixed-point architecture DSP, the square of the magnitude is used. Let $As(n) = (\bar{z}_1(n))^2 + (\bar{z}_2(n))^2$, where $\bar{z}_1(n)$ and $\bar{z}_2(n)$ are the averages of N samples of $z_1(k)$ and $z_2(k)$ $k = 0,1,2,\cdots,N_s$ $N \le N_s$, respectively. In order to discard the transients during one RF pulse, a starting point of averaging, N_0, is specified.

$$\bar{z}_1(n) = \frac{1}{N} \sum_{k=N_0}^{N_0+N-1} z_1(k), \tag{5.8}$$

$$\bar{z}_2(n) = \frac{1}{N} \sum_{k=N_0}^{N_0+N-1} z_2(k). \tag{5.9}$$

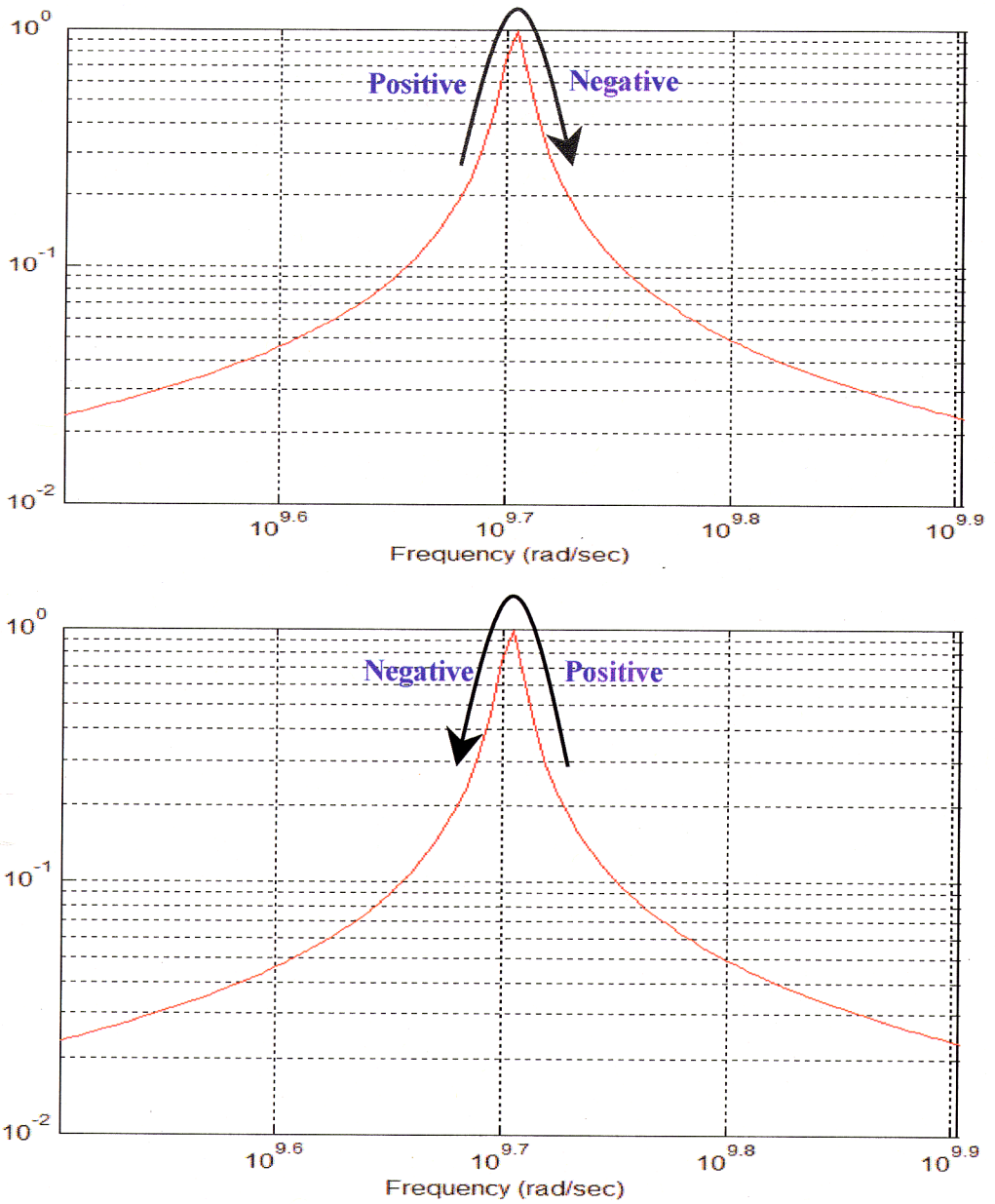

Figure 5.2. Directivity of Derivative (Difference) of the Magnitude Response of the Cavity Field with Respect to Frequency

An adaptive sweep-mode resonance controller is proposed where the frequency sweep amount is controlled by the adaptive gain. The generic adaptive sweep-mode resonance-controller algorithm is given by

Gain equation: $$\hat{G}(n+1) = \hat{G}(n) + sign\big(As(n) - As(n-1)\big)\cdot g\left(\frac{1}{\bar{z}_1^2(n) + \bar{z}_2^2(n)}\right) \tag{5.10}$$

Frequency Update : $$\Delta f(n) = \hat{G}(n)\Delta_f(n), \tag{5.11}$$

where $g(\cdot)$ is a continuous function and $\Delta_f(n)$ is the parameter related to the resolution of the frequency update, calculated at the nth RF pulse.

The gain-adaptation stop criterion can be introduced so that the adaptive gain (5.10) converges to a steady-state value. The simple rule can be found in Figure 5.1 or Figure 5.2. Around the resonance frequency, there is only a small change of magnitude. Within the 3-dB bandwidth of the cavity, there is a change of magnitude of 30%. Hence, a proper criterion is determined. A stop criterion for the gain adaptation can be expressed as

$$\big|As(n) - As(n-1)\big| \le \varepsilon_1, \tag{5.12}$$

where ε_1 is a design parameter, and the corresponding gain equation becomes

$$\hat{G}(n+1) = \hat{G}(n). \tag{5.13}$$

Another criterion is that

$$\frac{As(n)}{As(n-1)} \le \varepsilon_2, \tag{5.14}$$

where ε_2 is a design parameter. However, when (5.14) is used for the stop criterion, implementation is difficult because it is in the fixed-point DSP.

To avoid chattering around the resonance frequency, the parameter, Δ_f, is designed so that it changes its size as the number of the sign change of $As(n) - As(n-1)$ increases. We introduce a sign-change counter and assume that the sign-change counter has the number $c_n(n)$. Then, the parameter, Δ_f, is updated as

$$\Delta_f(n) = \frac{1}{c_n(n)+1}\Delta_f(n-1), \qquad c_n(0) = 0. \tag{5.15}$$

Note that when the frequency shift is large, that is, when $As(n)$ is very small, the proposed sweep-mode resonance control may have computational instability. In this case, rather than adapting the gain, a fixed gain is applied until $As(n)$ reaches sufficiently large value. This means that, in general, the proposed sweep-mode resonance control seems to work well when the frequency shift is within a few times of the 3-dB bandwidth of an SRF cavity.

When the frequency shift is so small that the phase rotation, $\Delta f(n)\cdot T_{RF}$, is less than 1, an adaptive sweep-mode resonance controller, given below, can be used where the direction of the frequency sweep is changed according to the sign change of the cavity field phase.

Gain equation: $$\hat{G}(n+1) = \hat{G}(n) + sign(\bar{z}_1(n)\bar{z}_2(n)) \cdot g\left(\frac{1}{\bar{z}_1^2(n) + \bar{z}_2^2(n)}\right) \tag{5.16}$$

Frequency update : $$\Delta f(n) = \hat{G}(n)\Delta_f(n) \tag{5.17}$$

To reflect the phase change at the resonance frequency, the *sign* function of the product, $\bar{z}_1(n)\bar{z}_2(n)$, of the I and Q of the cavity field is used

$$\tan(\phi_{CAV}(n)) = \frac{\bar{z}_2(n)}{\bar{z}_1(n)}. \tag{5.18}$$

Considering the tangent curve and noting that

$$\tan(\phi_{\text{detuning}}) = 2Q\frac{\Delta\omega}{\omega_o} = 2Q\frac{\Delta f}{f_o}, \tag{5.19}$$

$\phi_{CAV}(n)$ changes its sign when $\bar{z}_1(n)$ and $\bar{z}_2(n)$ have a different sign; that is, when $\bar{z}_1(n)\bar{z}_2(n)$ changes its sign. When the sign of the phase changes at the resonance frequency, the gain adaptation changes its direction (from negative to positive, or from positive to negative), and the corresponding frequency update also changes its direction.

A MATLAB/SIMULINK model was constructed to investigate adaptive sweep-mode resonance control. Figures 5.3–5.6 show the simulation results.

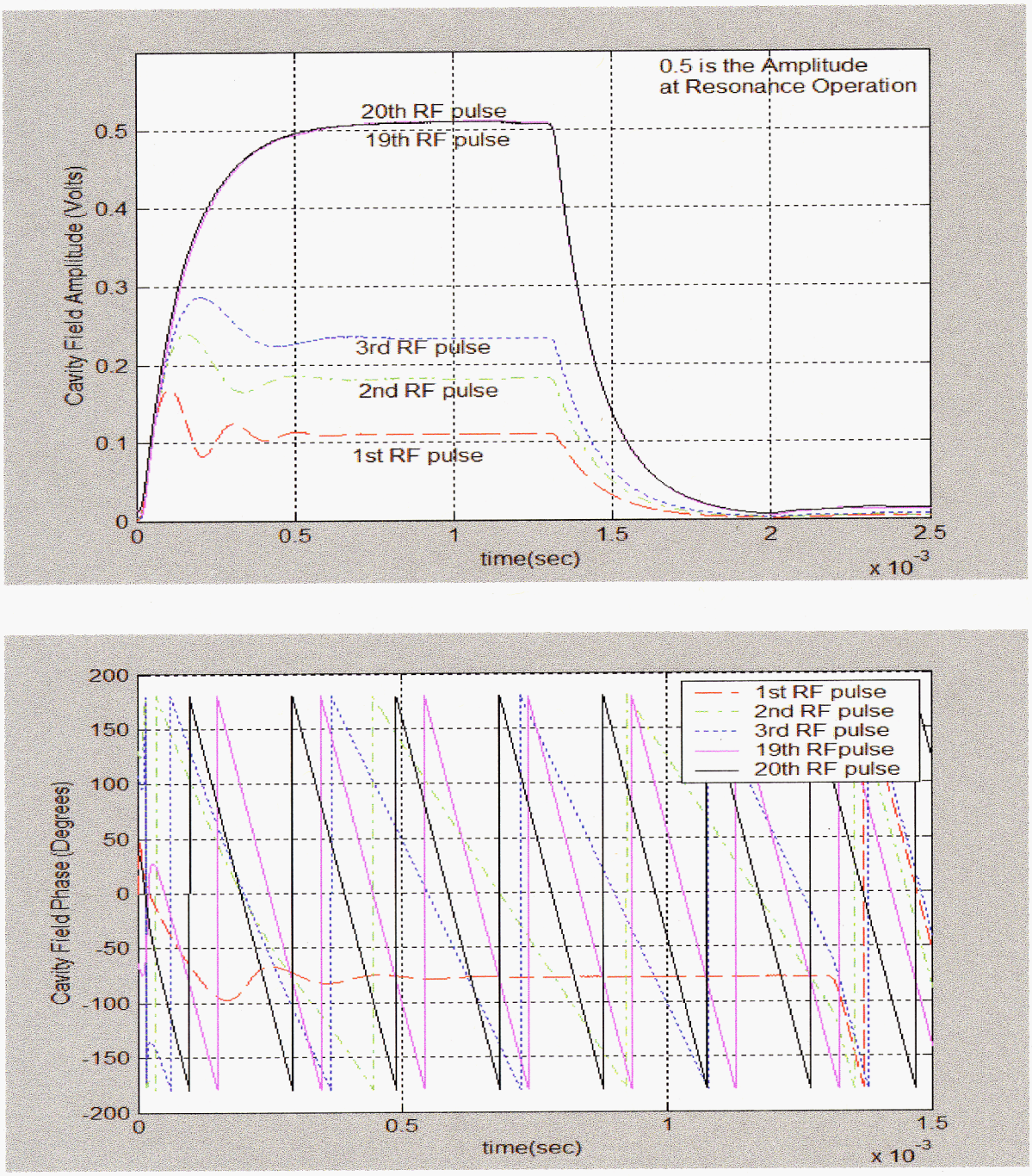

Figure 5.3. Cavity Field Amplitude (top) and Phase (bottom). The phase plot shows the phase modulation (phase rotation). The phase rotation increases as $\Delta f(n)$ increases. At the 20th RF pulse, $\Delta f(n)$ is 5.1 kHz (black line), and the phase rotation number is at its largest. At the 1st RF pulse, $\Delta f(n)$ is 0 and the phase rotation number is 0. The cavity field phase at this RF pulse is caused by frequency mismatch between the RF generator and the cavity.

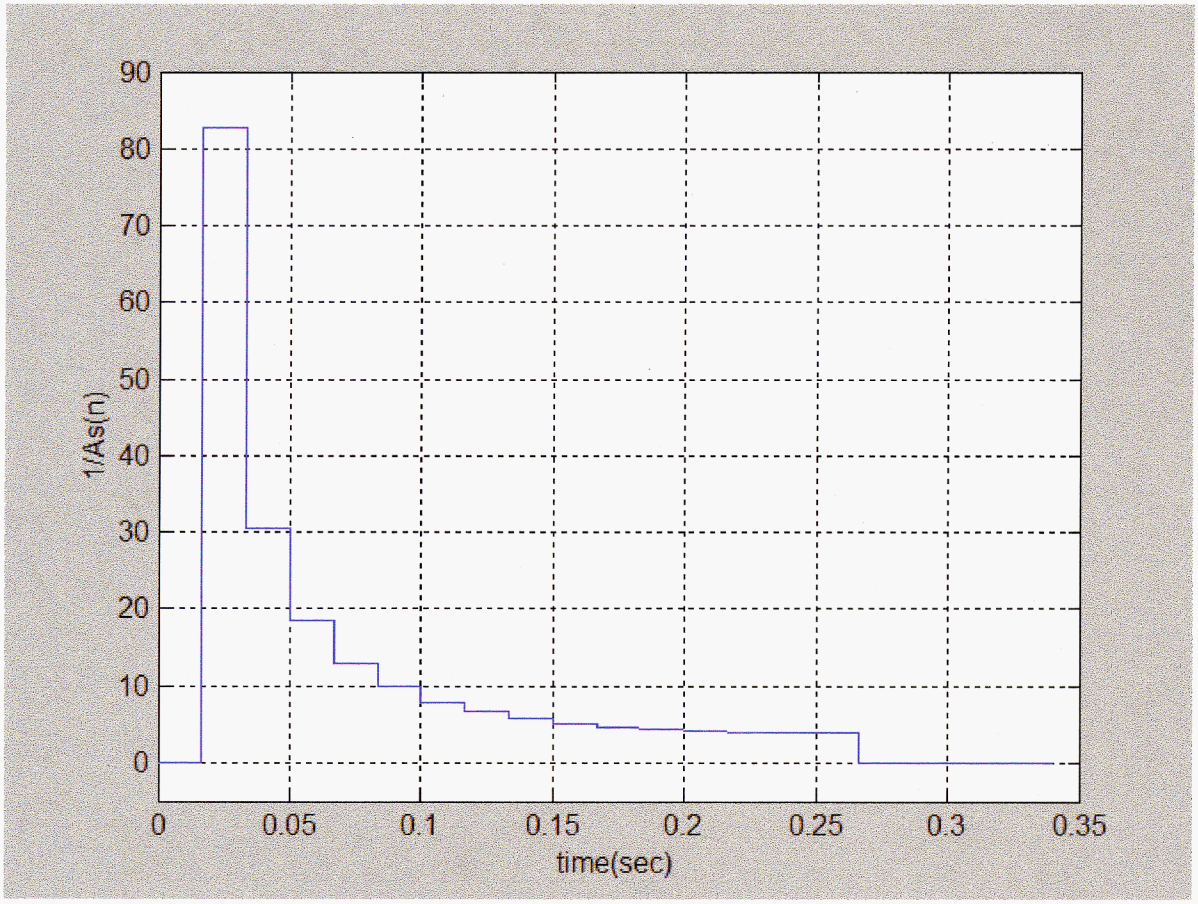

Figure 5.4. Inverse of the Square of Cavity Field Amplitude, $As(n)$

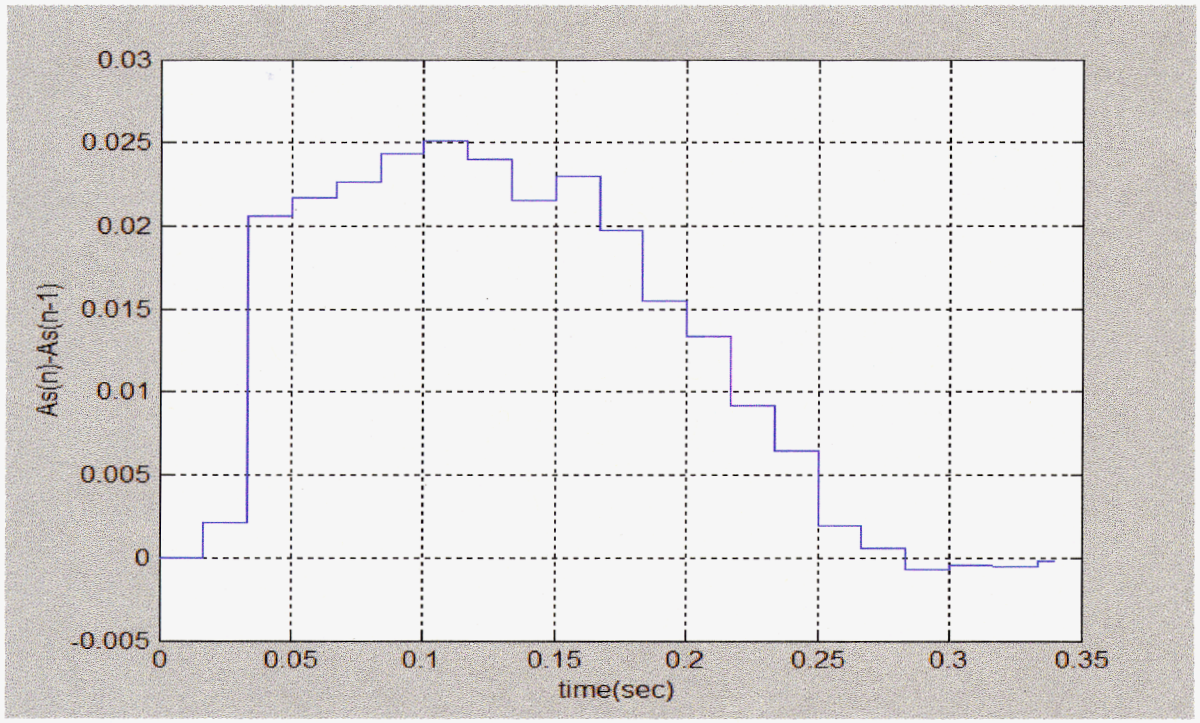

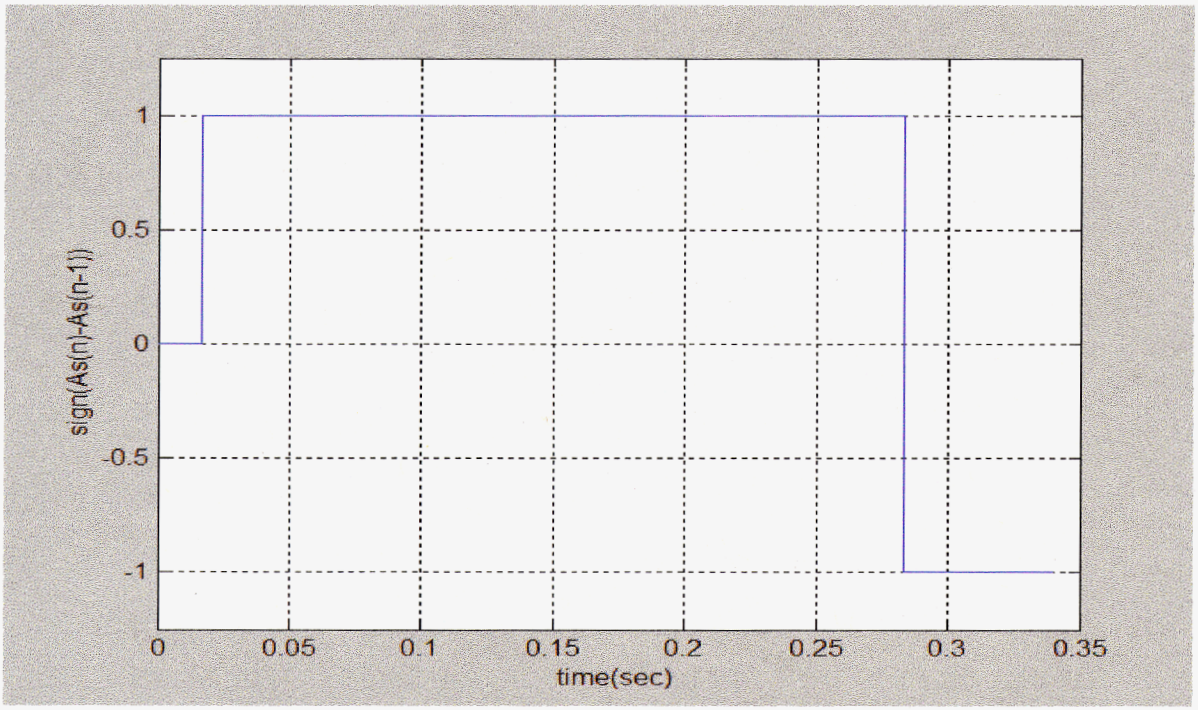

Figure 5.5. The Difference, $As(n) - As(n-1)$ (top), and Sign Function (bottom) of the Cavity Field Amplitude. This is used to check the sign change of the amplitude's derivative/difference.

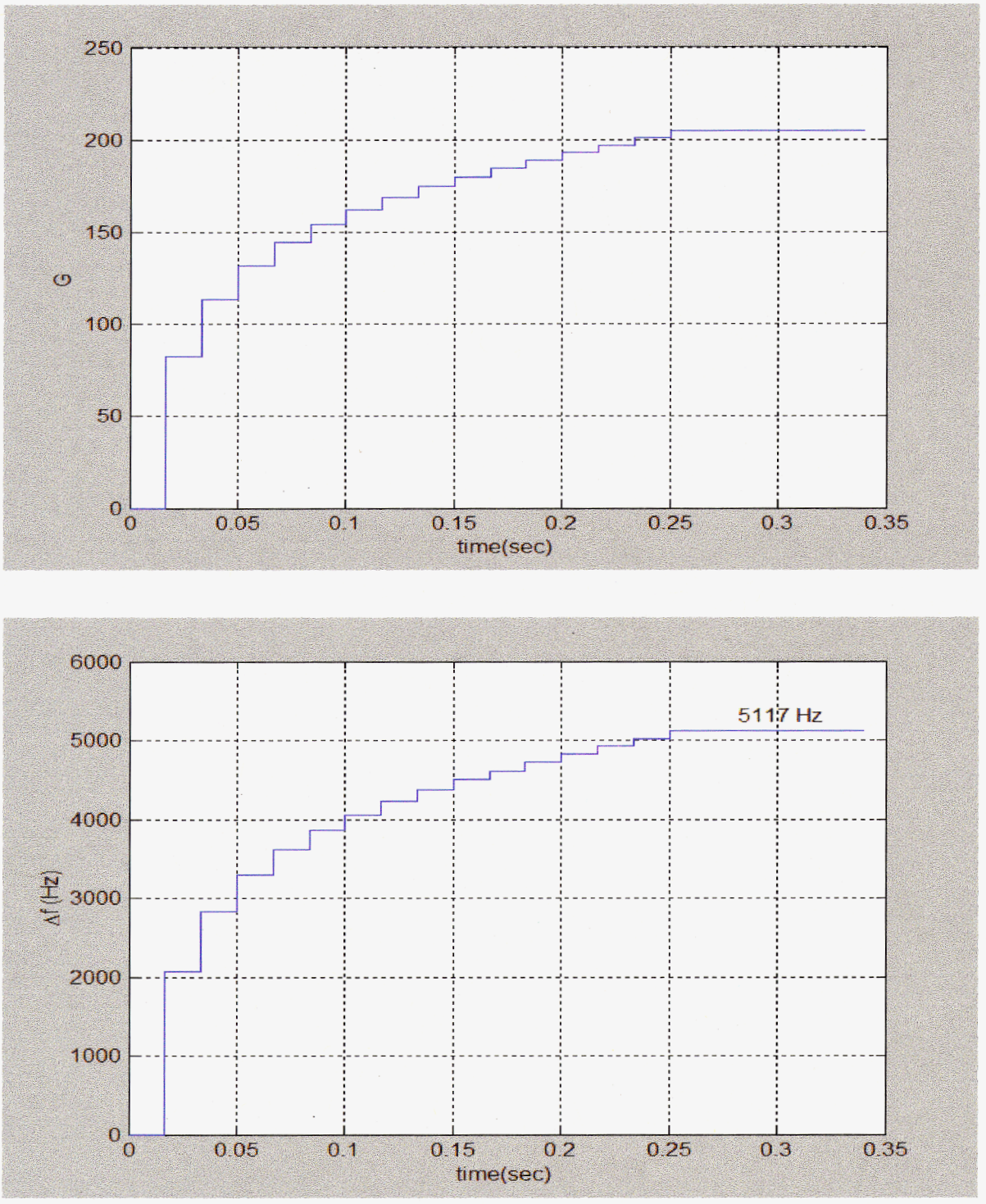

Figure 5.6. The Adaptive Gain Trajectory (top) and the Frequency-Shift Estimate Trajectory (bottom)

6. DIGITAL SIGNAL SYNTHESIS

DDS is used to generate a frequency- and phase-tunable output signal referenced to a fixed-frequency clock source by using digital data-processing blocks. In essence, the DDS architecture uses a scaling factor set forth in a programmable binary tuning word to divide down the reference clock frequency.

The output frequency of a DDS is determined by

$$F_{out} = \frac{M}{2^N} \cdot REFCLK, \tag{6.1}$$

where

M = the binary tuning word,

REFCLK = the internal reference clock frequency, and

N = the length, in bits, of the frequency accumulator.

The length, N, determines the resolution of the DDS.

Another function of the DDS is the phase-adjustment of the output signal. The amount of the adjustment is determined by the length of the phase-adjustment register bit. The amount of the phase-adjustment is given by

$$\theta = \frac{M_P}{2^{N_P}} \cdot 360^\circ, \tag{6.2}$$

where

M_P = the binary phase-adjustment register value, and

N_P = the length, in bits, of the phase-adjustment register.

When a 180° phase-adjustment is necessary, then M_P is

$$M_P = 2^{N_P - 1}.$$

The AD9852 digital synthesizer generates a highly stable frequency-phase-amplitude-programmable sine wave output. It has dual frequency accumulators and phase-adjustment registers. The length of the frequency accumulator is 48 bits and the phase-adjustment register, 14 bits. The maximum reference clock frequency is 300 MHz. Hence, the finest resolution of the output frequency is

$$\frac{300MHz}{2^{48}} \approx 1 \text{ μsec.} \tag{6.3}$$

The resolution of the phase-adjustment is

$$\frac{360^\circ}{2^{14}} = 0.022^\circ. \tag{6.4}$$

When a 180° phase-adjustment is necessary, then M_P is

$$M_P = 2^{13}. \tag{6.5}$$

Sometimes, the microHertz-level resolution is not necessary; for example, when the necessary frequency resolution is about 1 Hz. Then, the least-significant 20 bits of the frequency accumulator are filled with zeros and the rest of the bits are filled with the binary tuning word. In this case, the frequency resolution for a 300-MHz reference clock frequency is

$$\frac{2^{20}}{2^{48}} \cdot 300MHz \approx 1.1176 \text{ Hz}, \tag{6.6}$$

and the maximum output frequency that can be obtained is

$$2^{28} \approx 268 \text{ MHz}. \tag{6.7}$$

With this setup, to generate 30 kHz, the binary tuning word, M, is

$$26843\,(68\mathrm{DB}_h) \times 2^{20}, \tag{6.8}$$

and the frequency accumulator is shown in Figure 6.1.

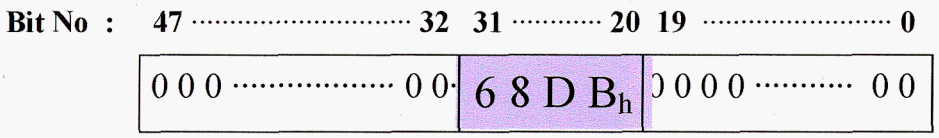

Figure 6.1 DDS AD9852 Frequency Accumulator

6.1 Coupling Between the DDS and the DSP

Consider the DSP that will be used. The TMS320C6203B 32-bit DSP is used for the SNS frequency-control system. As addressed in the previous section, DDS resolution is assumed to be 1.1176 Hz.

There are four inputs to the frequency-control software module: V_{FI}, V_{FQ}, V_{TI}, V_{TQ}. The arrays of these are stored in the external RAM of the DSP TMS320C6203B in 16-bit Q15-format, and are retrieved through direct memory access (DMA). Hence, the error $e(n)$ calculated from these data, V_{FI}, V_{FQ}, V_{TI}, and the corresponding frequency, $\Delta f(n)$, can be either 16-bit Q15-format or 32-bit integer format. Considering the compatibility between the structure of the DDS frequency accumulator and the data structure of the DSP, $e(n)$ and $\Delta f(n)$ are in 32-bit integer format. DSP data 0x00000001 represents 1.1176 Hz.

There are two 32-bit registers in the complex programmable logic device (CPLD). The first 32-bit register (DDS_FREQ_TUNE_LOW) is for the lower 32 bits of the frequency accumulator of the DDS. The second 32-bit register (DDS_FREQ_TUNE_HIGH) is for the other 16 bits of the frequency accumulator. Both registers are defined as unsigned integer formats. Two steps are required to load the 32-bit frequency data, $\Delta f(n)$, to the 48-bit frequency accumulator of the DDS. The first step is to shift the 32-bit integer data, $\Delta f(n)$, 20 bits to the left. That shifted data is then loaded to the CPLD register DDS_FREQ_TUNE_LOW. The high 20 bits of the 32-bit integer data, $\Delta f(n)$, need to be loaded to the CPLD register DDS_FREQ_TUNE_HIGH; therefore, in the second step, the 32-bit integer data, $\Delta f(n)$, is shifted 12 bits to the right, and the shifted data is loaded to DDS_FREQ_TUNE_HIGH. These loading schemes are summarized in Figure 6.2. As a result, the output frequency range is $[1.1176\ Hz \quad 300\ MHz\ ]$.

The 32-bit integer data, $\Delta f(n)$, is the driving RF frequency update value. In the hardware, $\Delta f(n)$ is added to 50 MHz. The local oscillator (LO) frequency of the I/Q modulator is f_{LO}. Because DSP data 0x00000001 represents 1.1176 Hz, 50 MHz is represented by 0x02AAA8A6 (44738726 in decimal). Hence, the LO frequency is $\Delta f(n)$ +0x02AAA8A6, which is the output of the DDS.

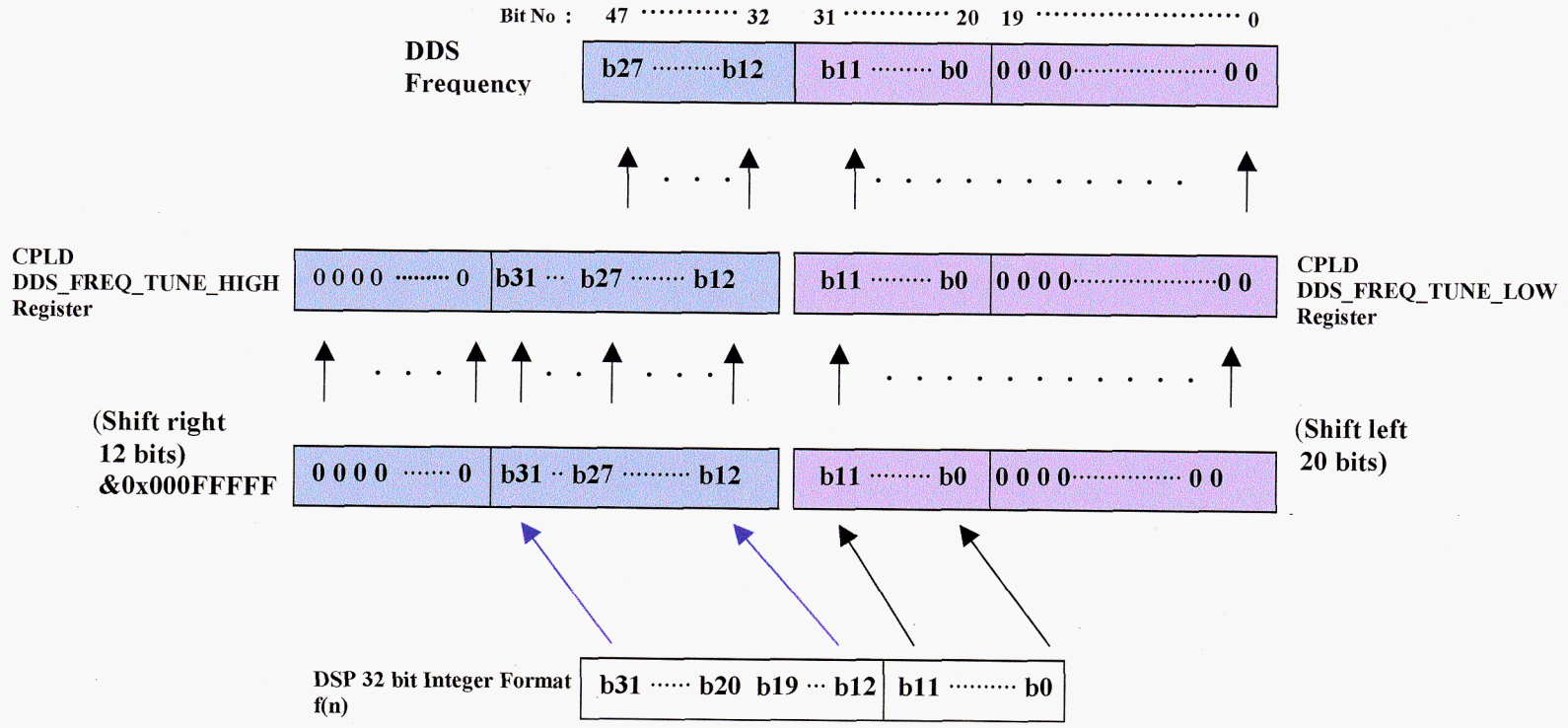

Figure 6.2. DDS AD9852 Frequency Accumulator Frequency Tuning Word Loading Scheme

For example, when the driving RF frequency update, $\Delta f(n)$, is 30 kHz, the corresponding DSP 32-bit integer-format data is 0x000068DB (26843 in decimal). Hence, the DSP data, including 50 MHz, is 0x02AB1181 (44765569 in decimal), as shown in Figure 6.3.

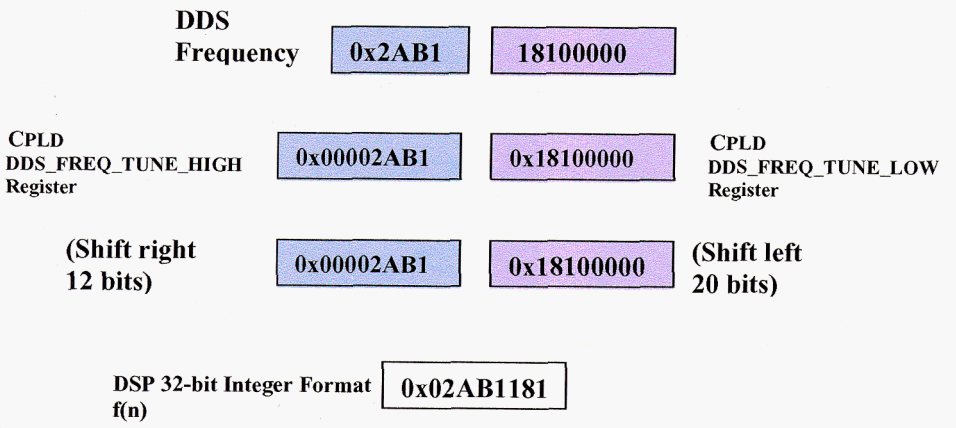

Figure 6.3. DDS AD9852 Frequency Accumulator Frequency Tuning Word Loading Example. The output frequency of the DDS is 20 kHz + 50 MHz, which is represented by 0x02AB1181 (44765569 in decimal).

7. DMA

In the frequency-control algorithm, there should be burst data transfer between the external memory interface (EMIF) asynchronous burst SRAM, the DSP internal data RAM, the VXI interface dual-port RAM, and the cavity-field dual-port RAM. Because the data stored during the RF pulse ON is massive due to the 20-MHz sampling frequency for each analog signal channel, huge data-memory spaces are necessary. For the 1.1 msec RF ON period in the normal-conducting cavity, we need to sample the cavity-field error and forward signal.

The cavity-field signal and the forward signal of the current RF pulse period are stored in the cavity dual-port RAM and the forward-signal dual-port RAM, respectively. These data need to be transferred to the DSP's internal data RAM because the field- and resonance-control module (FRCM) for SNS has two TMS320C6203 DSPs, one for field control and the other for resonance control (frequency control). Both share the same address bus and data bus; therefore, there may be conflicts when both DSPs have access to the data bus because data that is requested by one DSP may be retrieved to the other DSP. Hence, the cavity signal and the forward signal in dual-port RAM must be transferred to the internal RAM via DMA.

For diagnostic purposes, the data stored in the history buffer (FIFO) needs to be transferred to the 16-bit little endian VXI dual-port RAM. Full-size data is not needed for diagnosis (in the case of the 20-MHz and 1.1-msec RF ON period, 22000 samples of each signal will suffice). Instead, decimated data is to be transferred to the VXI dual-port RAM. This decimation and massive data transfer requires DMA.

8. MEMORY MAPS

The TI DSP TMS320C6203B has a 512-kbyte internal data RAM and supports four EMIFs, CE0, CE1, CE2, and CE3. SNS will use the external memory maps shown in the following tables. Table 8.1 shows the memory map for DSP A (field control) and Table 8.2 shows the memory map for DSP B (resonance control).

Table 8.1. DSP A, Field-Control DSP

	Address Range	Size (Bytes)	Descriptions
CE0 32-bit little endian	0x00400000-0x005F FFFF	2M	Asynchronous Burst SRAM
	0x00600000-0x007FFFFF	2M	Reserved
	0x00800000-0x013FFFFF	12M	Not Accessible
CE1 32-bit little endian	0x01400000-0x015FFFFF	2M	Flash Memory
	0x01600000-0x017FFFFF	2M	Reserved
CE2 16-bit little endian	0x02000000-0x0200FFFF	64K	VXI Control/Status Registers
	0x02010000-0x0204FFFF	256K	VXI Dual-Port RAM
	0x02050000-0x023FFFFF	4M–320K	Reserved
	0x02040000-0x02FFFFFF	12M	Not Accessible
CE3 32-bit little endian	0x03000000-0x0300FFFF	64K	Control/Status Registers
	0x03010000-0x0304FFFF	256K	DSP B Dual-Port RAM
	0x03050000-0x0308FFFF	256K	NIOS Dual-Port RAM
	0x03090000-0x030AFFFF	128K	Cavity Error PLD Dual-Port RAM
	0x030B0000-0x030CFFFF	128K	Beam PLD Dual-Port RAM
	0x030D0000-0x033FFFFF	3M–832K	Reserved
	0x03400000-0x03FFFFFF	12M	Not Accessible

Table 8.2. DSP B, Resonance-Control DSP

	Address Range	Size (Bytes)	Descriptions
CE0 32-bit little endian	0x00400000- 0x005F FFFF	2M	Asynchronous Burst SRAM
	0x00600000-0x007FFFFF	2M	Reserved
	0x00800000-0x013FFFFF	12M	Not Accessible
CE1 32-bit little endian	0x01400000-0x015FFFFF	2M	Flash Memory
	0x01600000-0x017FFFFF	2M	Reserved
CE2 16-bit little endian	0x02000000-0x0200FFFF	64K	VXI Control/Status Registers
	0x02010000-0x0204FFFF	256K	VXI Dual-Port RAM
	0x02050000-0x023FFFFF	4M–320K	Reserved
	0x02040000-0x02FFFFFF	12M	Not Accessible
CE3 32-bit little endian	0x03000000-0x0300FFFF	64K	Control/Status Registers
	0x03010000-0x0304FFFF	256K	DSP A Dual-Port RAM
	0x03050000-0x0308FFFF	256K	NIOS Dual-Port RAM
	0x03090000-0x030AFFFF	128K	Cavity PLD Dual-Port RAM
	0x030B0000-0x030CFFFF	128K	Forward PLD Dual-Port RAM
	0x030D0000-0x030EFFFFF	128K	Reflected PLD Dual-Port RAM
	0x030F0000-0x033FFFFF	3M–960K	Reserved
	0x03400000-0x03FFFFFF	12M	Not Accessible

9. TMS320C6203B DMA STRUCTURE

The TMS320C6203B DSP has four independent DMA channels (shown in Figure 9.1), and each channel has its own burst FIFO. These are able to co-exist without loss of throughput (1.5 V devices).

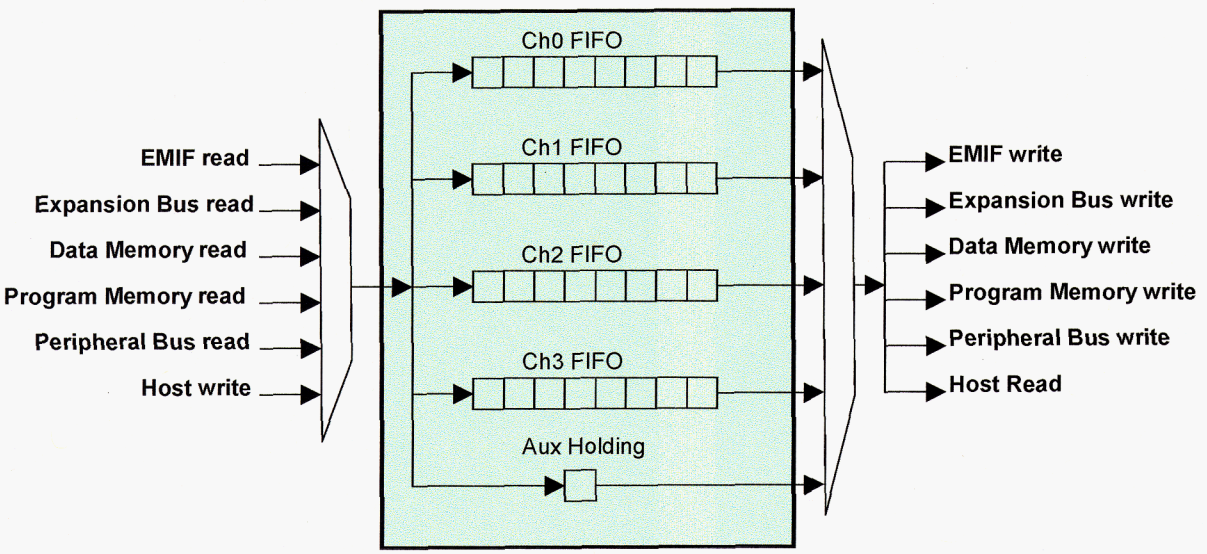

Figure 9.1. DMA Controller Data Bus Block Diagram for 1.5 V Device

Each channel has a dedicated 9-deep FIFO to facilitate bursting to high-speed memories. Each channel has its own FIFO, which reduces the arbitration required for switching between high-speed bursting channels. The individual operation by any channel is unchanged by any other channel. The benefit of multiple FIFOs comes into play only when switching channels.

10. DMA STRATEGY

10.1 DMA #1: DMA for Cavity Field

The cavity-field data of the RF pulse period, which is stored in the cavity-field dual-port RAM, must be transferred into the field-control DSP's internal data memory to update the current feedforward-control output corresponding to the current Pulse ID. The source of the DMA is the dual-port RAM, and the destination is the internal data memory. Figure 10.1 shows the structure of the I and Q error data stored in the dual-port RAM. The following is the simplest way to achieve DMA:

Primary Control Register

1) CPU interrupt after block move completion
2) No read synchronization
3) No write synchronization
4) **Element Size:** 32 bit
5) **Source Direction**: increment of address by element size (4 bytes)
6) **Destination Direction**: increment of address by element size (4 bytes)
7) **Source Address**: 0x03090000
8) **Destination Address**: DMA_no_1_desBuffer, which is the buffer (array) assigned in the internal data memory

Transfer Counter Register

9) **Frame size**: 0
10) **Element Count**: RF ON period (sec)*Sampling Frequency (Hz). Default value: 22000

Figure 10.1. Cavity-field Dual-Port RAM Data Structure

When the computation of the feedforward-control output has been updated, the transferred data should be decomposed into two Q15-format I error and Q error data.

Figure 10.2 shows the simulation result of composing transmitted I and Q signals into a single 32-bit integer.

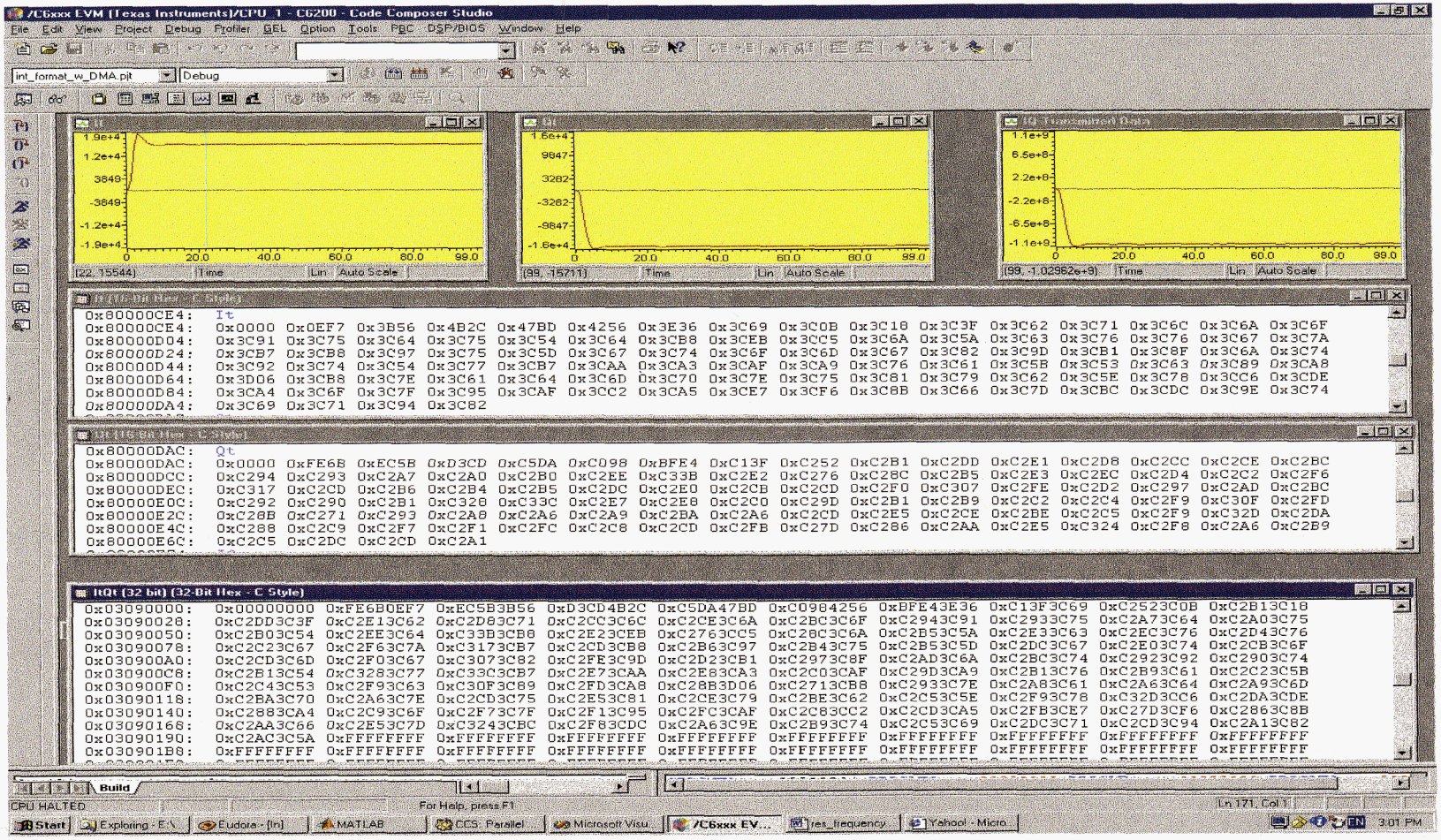

Figure 10.2. A module, IQCompose(short Idata, short *Qdata)*, is developed to compose one signed integer data from two signed short data. This figure shows the simulation result, with the TMS320C6201EVM, of composing a transmitted I signal (I_t) and a transmitted Q signal (Q_t) into a 32-bit integer.

10.2 DMA #2: DMA for Forward Signal

The forward-signal data of the RF pulse period, which is stored in the forward-signal dual-port RAM, must be transferred into the resonance-control DSP's internal data memory to update the resonance frequency control. The source of the DMA is the dual-port RAM, and the destination is the internal data memory. Figure 10.3 shows the structure of the I and Q error data stored in the dual-port RAM. The following is the simplest way to achieve DMA:

Primary Control Register

11) CPU interrupt after block move completion
12) No read synchronization
13) No write synchronization
14) **Element Size:** 32 bit
15) **Source Direction**: increment of address by element size (4 bytes)
16) **Destination Direction**: increment of address by element size (4 bytes)
17) **Source Address**: 0x030B0000
18) **Destination Address**: DMA_no_1_desBuffer, which is the buffer (array) assigned in the internal data memory

Transfer Counter Register

19) **Frame size**: 0
20) **Element Count**: RF ON period (sec)*Sampling Frequency (Hz). Default value: 22000

Figure 10.3. Cavity-Error Dual-Port RAM Data Structure

Figure 10.4 shows the simulation result of composing forward I and Q signals into a single 32-bit integer.

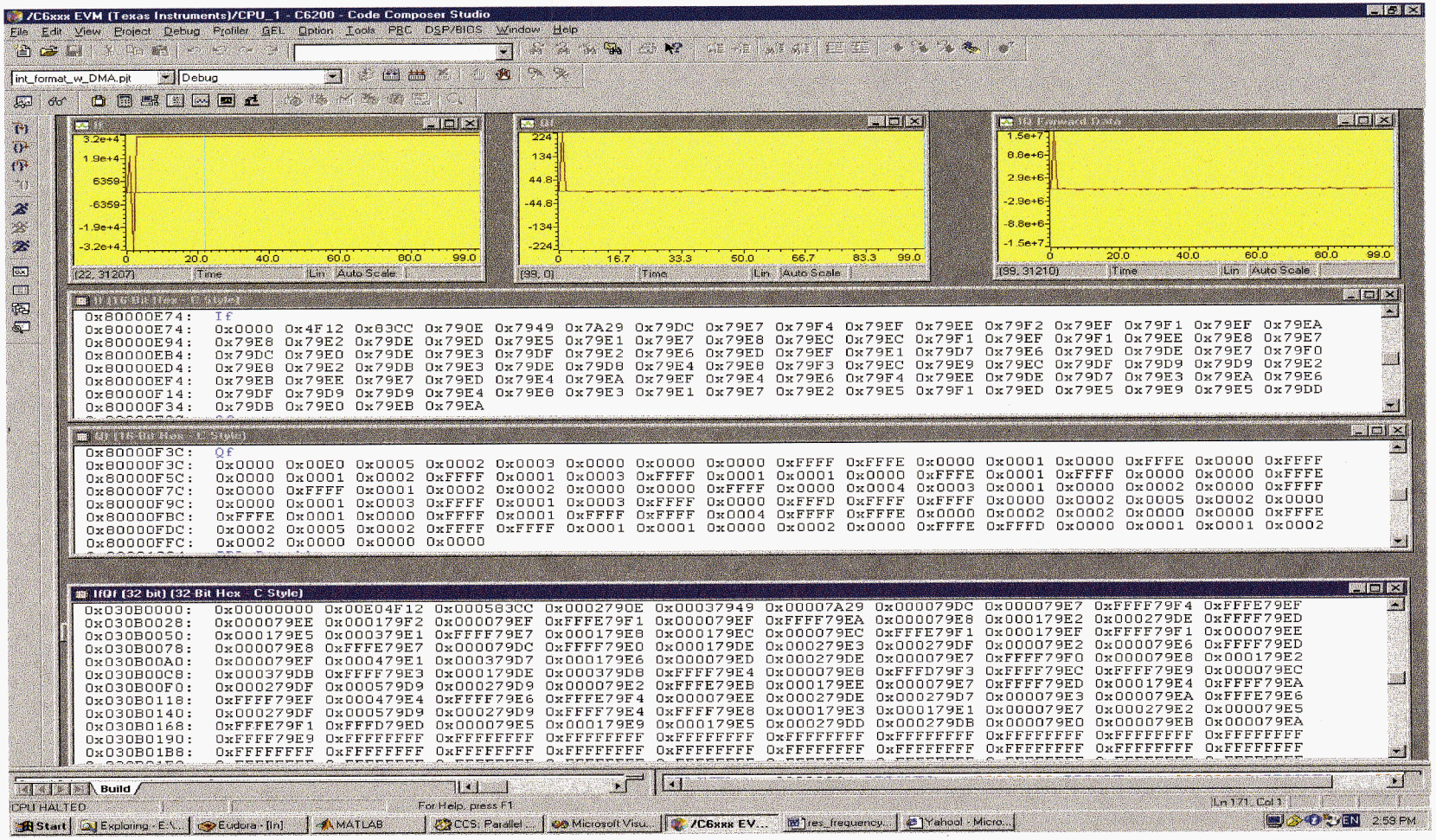

Figure 10.4. A module, IQCompose(short Idata, short *Qdata)*, is developed to compose one signed integer data from two signed short data. This figure shows the simulation result, with the TMS320C6201EVM, of composing a forward I signal (I_f) and a forward Q signal (Q_f) into a 32-bit integer.

10.3 DMA #3: DMA for Cavity-field 1 History Buffer (FIFO)

The field data for cavity 1 is stored as FIFO 32-k RAM during the RF ON period. For diagnosis, this data is transferred to EPICS through VXI. The data is transferred to the VXI dual-port RAM, and is then retrieved by the host (EPICS). In general, whole data samples are not necessary, and a data decimation is given by the host. The DSP reads the decimation number, which is transferred from the host to a VXI register in the CPLD. This decimation number is used for setting the DMA. The FIFO is a 32-bit little endian and the VXI dual-port RAM is a 16-bit little endian; this determines the element size of the DMA. Because it is impossible to reflect the decimation with FIFO RAM, the data in FIFO is first transferred to the temporary memory space in the DSP's internal data memory and then the DMA is set to reflect the decimation, which is programmed with Global Index Register A or B. Figure 10.5 illustrates this process.

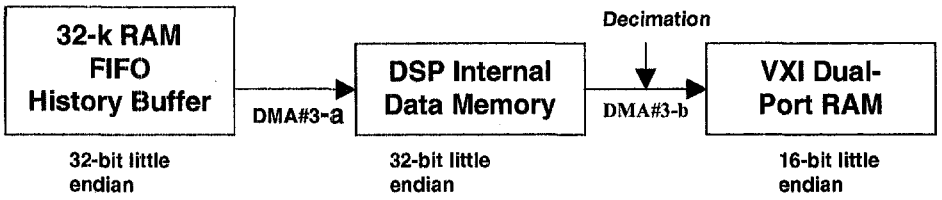

Figure 10.5. History Buffer Data DMA Scheme (Cavity field of Cavity 1)

The DMA #3-a has the following parameter setup

Primary Control Register

1) CPU interrupt after block move completion
2) No read synchronization
3) No write synchronization
4) **Element size** :32 bit
5) **Source Direction**: no modification
6) **Destination Direction**: increment of address by element size (4 bytes)
7) **Source Address**: 0x0300000C, which is given in CPLD cavity control/status register memory maps

8) **Destination Address**: DMA_no_3_desBuffer, which is the buffer (array) assigned in the internal data memory

Transfer Counter Register

9) **Frame size**: 0

10) **Element Count**: RF on period (sec)*Sampling Frequency (Hz). Default value:22000

DMA #3-b needs special care. Figure 10.6 shows an example where 84 32-bit data (I(Q15) and Q(Q15)) are in the DSP's internal data memory, and the decimation number is 4 in words. The following conditions are in effect in this example:

a) the element size is to be 16 bits (ESIZE=01b in primary control register),

b) the frame count is 21 (=84/4),

c) the element count in each frame is 2,

d) the frame index, representing the address adjustment in bytes between the start address of the last element of one frame and the start address of the next adjacent frame, is 14(=decimation number*4-2) bytes, and

e) the element index representing the address adjustment in bytes between two adjacent elements in a frame (i.e., the address difference in bytes between two start addresses of two adjacent elements in a frame) is 2 bytes.

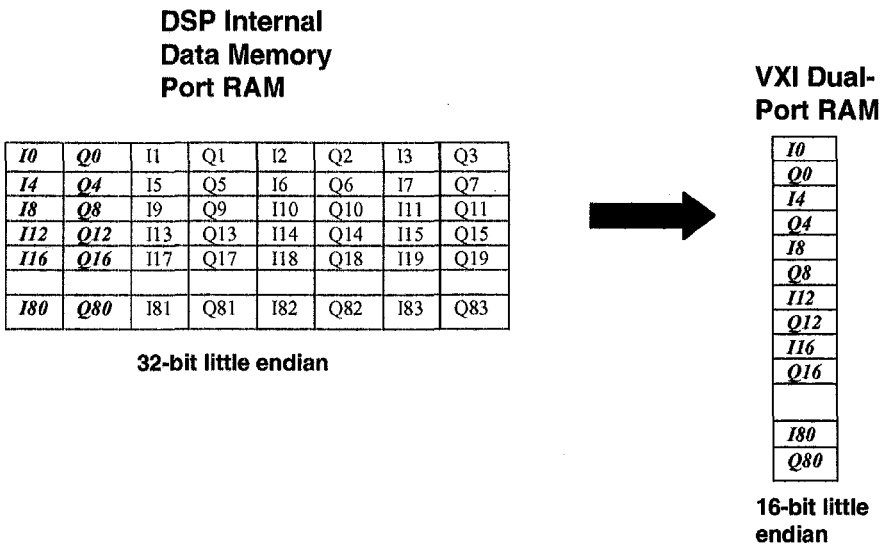

Figure 10.6. Example of DMA Between the DPS Internal Data Memory and the VXI Dual-Port RAM.

The above example is generalized for the arbitrary number of data in words and the decimation number in words, which results in the following parameter setup (DMA#3-b):

Primary Control Register

1) CPU interrupt after block move completion
2) No read synchronization
3) No write synchronization
4) **Element Size:** 01b (16 bit)
5) **Source Direction**: 11b, which represents the address modification is programmed by using Global Index Register
6) **Destination Direction**: 01b (increment of address by element size [2 bytes])
11) **Source Address**: DMA_no_3_desBuffer, which is the buffer (array) assigned in the internal data memory
7) **Destination Address**: 0x02010000, which is in CE1 of the DSP B memory maps.
8) **Primary Control Register INDEX bit**: 0b, representing Global Index Register A

Transfer Counter Register

9) **Frame size**: *(Data number in words)/(Decimation number in words)*
10) **Element Count**: 10b (2)

Global Index Register A

11) **Frame Index in bytes**: *(Decimation number in words)× 4-2*
12) **Element Index in bytes**: 2

10.4 DMA #4: DMA for Cavity-field 2 History Buffer (FIFO)

The same DMA scheme is used, except for the source addresses and the destination addresses (as shown in Figure 10.7).

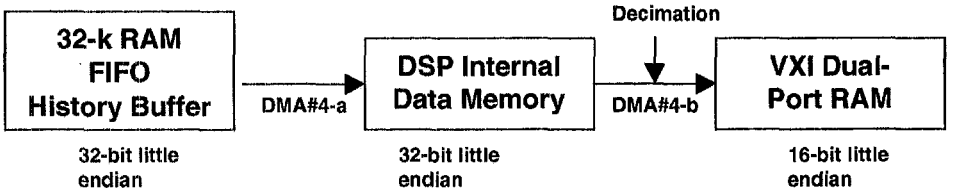

Figure 10.7. History Buffer Data DMA Scheme (Cavity Field of Cavity 2)

DMA #4-a has the following parameter setup:

Primary Control Register

1) CPU interrupt after block move completion
2) No read synchronization
3) No write synchronization
4) **Element Size:** 32 bit
5) **Source Direction**: increment of address by element size (4 bytes)
6) **Destination Direction**: increment of address by element size (4 bytes)
7) **Source Address**: 0x03000010, which is given in CPLD cavity control/status register memory maps
8) **Destination Address**: DMA_no_4_desBuffer, which is the buffer (array) assigned in the internal data memory

Transfer Counter Register

9) **Frame size**: 0
10) **Element Count**: RF ON period (sec)*Sampling Frequency (Hz). Default value: 22000

DMA#4-b has the following parameter setup:

Primary Control Register

1) CPU interrupt after block move completion
2) No read synchronization
3) No write synchronization
4) **Element Size:** 01b (16 bit)
5) **Source Direction**: 11b, which represents the address modification is programmed by using Global Index Register
6) **Destination Direction**: 01b (increment of address by element size [2 bytes])
7) **Source Address**: DMA_no_4_desBuffer, which is the buffer (array) assigned in the internal data memory
8) **Destination Address**: 0x02030000, which is in CE1 of the DSP B memory maps.
9) **Primary Control Register INDEX bit** : 0b, representing Global Index Register A
10) ***Transfer Counter Register***
11) **Frame size**: *(Data number in words)/(Decimation number in word)*
12) **Element Count**: 10b (2)
13) ***Global Index Register A***

14) **Frame Index in bytes**: *(Decimation number in words)×4-2*

15) **Element Index in bytes**: 2

10.5 DMA #5: DMA for Set-Point-Profile Load

When the single beam-current profile is considered, the set-point profile can be calculated at the initialization module or during the RF pulse OFF period. However, when eight beam-current profiles are considered, memory space availability becomes an issue. The current hardware design shows that the asynchronous SRAM space in CE0 is enough for both the feedforward-control-output table and the set-point-profile table. The same rule is applied to the calculation of the memory assignment for the set-point-profile table as for the feedforward-control-output table. For the 1.1-msec RF pulse ON period and the 20-MHz sampling frequency, 88 kbytes are necessary to store I and Q set-point profiles for one beam-current profile. Hence, for eight beam-current profiles, 704 kbytes of memory space is necessary. The second 1 Mbyte of the 2-Mbyte asynchronous SRAM is assigned to store the set-point-profile table, as shown in Table 10.1.

Table 10.1. Set-Point-Profile Table Memory Allocation

Pulse ID	Set-Point Profile (32 bit)	Start Address	Size (Bytes)
0	SP0	0x00500000	128 K
1	SP1	0x00520000	128 K
2	SP2	0x00540000	128 K
3	SP3	0x00560000	128 K
4	SP4	0x00580000	128 K
5	SP5	0x005A0000	128 K
6	SP6	0x005C0000	128 K
7	SP7	0x005E0000	128 K

The set-point profiles for eight beam-current profiles are computed at the initialization module and are stored in asynchronous SRAM. The data structure of each address is shown in Figure 10.8.

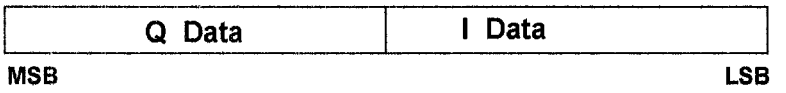

Figure 10.8. Set-Point-Profile Asynchronous SRAM Data Structure

To compute the set-point profile, we need to know the beam-current amplitude and the beam ON period. This data comes from EPICS. Other information, such as the cavity-filling time and the premargin are fixed. For a normal-conducting cavity, the filling time is 100 μsec and the premargin is 20 μsec. For an SRF cavity, the filling time is 300 μsec and the premargin is 20 μsec. Figure 10.9 shows the timing diagram of the set-point profile, the beam current, and the RF gate for an SRF cavity.

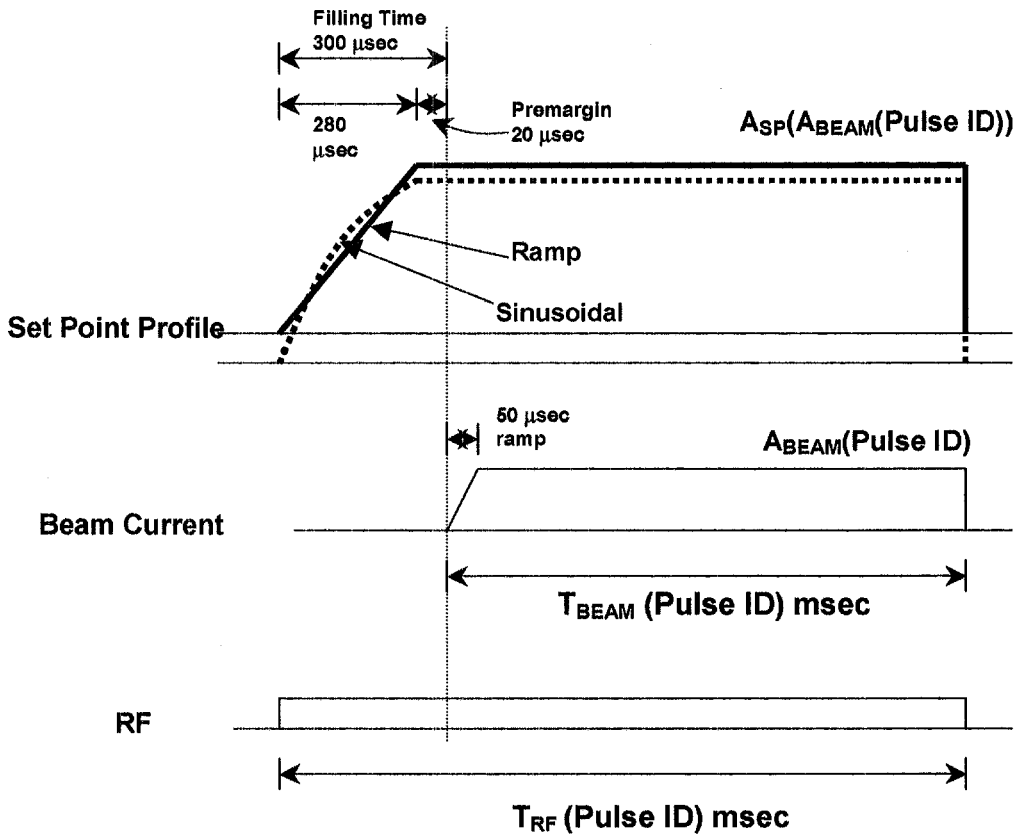

Figure 10.9. Timing Diagram of the Set-Point Profile, the Beam Current, and the RF Gate. One candidate for the set-point turn-on is ramp, and the other is sinusoidal during the filling time. The beam-pulse period and the RF gate period are functions of Pulse ID. Also, set-point amplitude, A_{SP}, beam-current amplitude, and A_{BEAM}, are functions of Pulse ID.

To compute the set-point profile with the DSP, the timing diagram of the set-point profile, shown in Figure 10.9, should be converted to the discrete-time domain. Note that the sampling frequency is 20 MHz. Figure 10.10 shows the result for the set-point profile with ramp. The magnitude $A_{SP}(A_{BEAM}(\text{Pulse ID})$ is represented in Q15 format. The sample numbers N_F, N_{PM}, and $N_{BEAM}(\text{Pulse ID})$ correspond to 280 μsec, 20 μsec, and $T_{BEAM}(\text{Pulse ID})$, respectively.

$$N_F = 280e^{-6} \times 20e^6 = 5600 \text{ (samples)}$$

$$N_{PM} = 20e^{-6} \times 20e^6 = 400 \text{ (samples)}$$

$$N_{BEAM}(PulseID) = T_{BEAM}(PulseID) \times 20e^6 \text{ (samples).}$$

Also, the slope of the ramp is

$$slope = \frac{A_{SP}(A_{BEAM}(PulseID))}{N_F}.$$

Based on the above equations, the set-point profile corresponding to Pulse ID is calculated and stored in asynchronous SRAM.

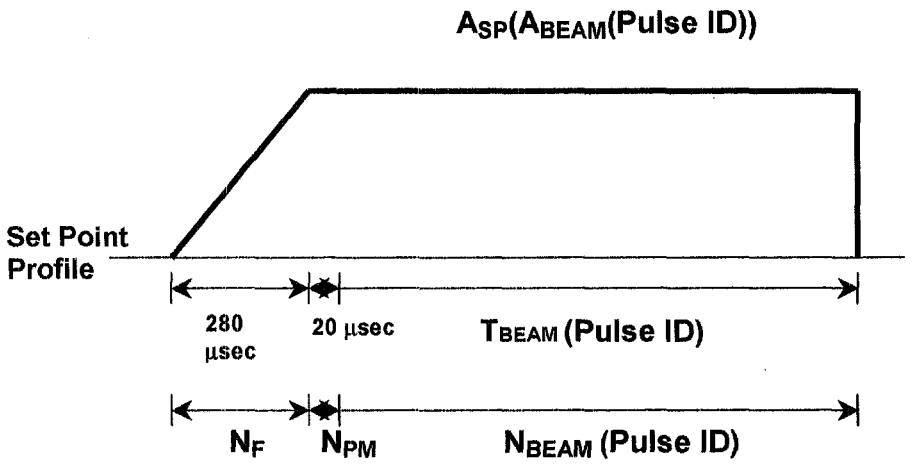

Figure 10.10. Timing Diagram of the Set-Point Profile in Discrete-Time Domain

When the prepulse arrives, along with the Pulse ID, the corresponding set-point profile is transferred, via DMA, to a 32-k RAM set-point FIFO. The following are the important DMA parameters:

Primary Control Register

1) CPU interrupt after block move completion
2) No read synchronization
3) No write synchronization
4) **Element Size:** 32 bit
5) **Source Direction**: increment of address by element size (4 bytes)
6) **Destination Direction**: no modification
7) **Source Address:** 0x00500000+(Next Pulse ID)*0x00020000,
   Next Pulse ID=0,1,2,3,4,5,6,7
8) **Destination Address**: 0x03000014

Transfer Counter Register

9) **Frame size**: 0
10) **Element Count**: RF ON period (sec)*Sampling Frequency (Hz). Default value: 22000

11. GROUPING OF DMAS TO IMPROVE THROUGHPUT

Thus far, several DMA schemes have been addressed. To improve the throughput, the DMAs are grouped appropriately. Figure 11.1 shows the grouping. Table 11.1 summarizes the various DMA schemes.

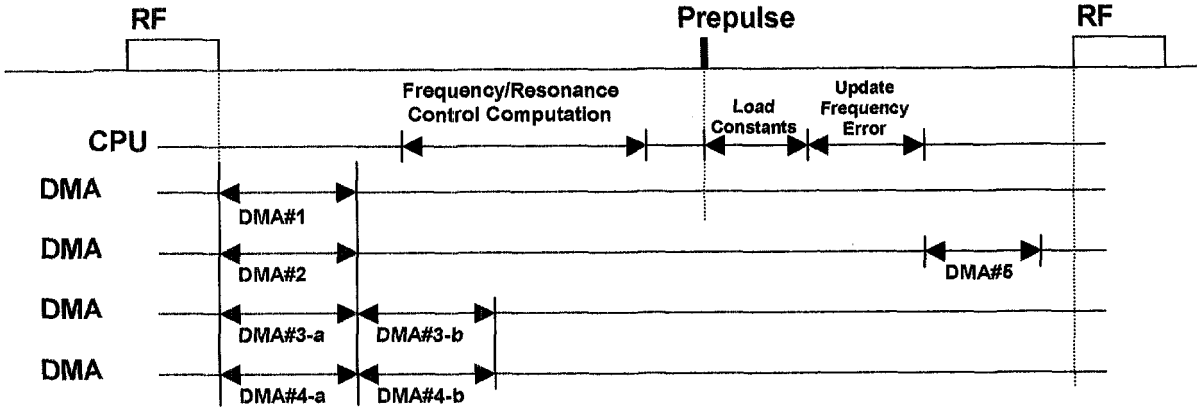

Figure 11.1. DMA Grouping to Improve Performance

Table 11.1. DMA Summary

DMA no	DMA Channel	Primary Control Register	Secondary Control Register	Transfer Counter Register	Source Address	Destination Address	Global Index Register
1 **Cavity Field**	**0**	0x03000050	0x00000080	0x0000 ----	0x03090000 (Cavity-Field Dual-Port RAM)	DMA_no_1_desBuffer (Internal Data Memory)	0x00000000
2 **Forward Signal**	**1**	0x03000050	0x00000080	0x0000 ----	0x030B0000 (Forward-Signal Dual-Port RAM)	DMA_no_2_desBuffer (Internal Data Memory)	0x00000000
3-a **History Buffer 1**	**2**	0x03000040	0x00000080	0x0000 ----	0x0300000C (32 k Cav 1 HB FIFO)	DMA_no_3a_desBuffer (Internal Data Memory)	0x00000000
4-a **History Buffer 2**	**3**	0x03000040	0x00000080	0x0000 ----	0x03000010 (32k Cav 2 HB FIFO)	DMA_no_4a_desBuffer (Internal Data Memory)	0x00000000
3-b	**2**	0x03000170	0x00000080	0x00C8 0002	DMA_no_3a_desBuffer (Internal Data Memory)	0x02010000 (VXI Dual-Port RAM)	0xYYYY 0002
4-b	**3**	0x03000170	0x00000080	0x00C8 0002	DMA_no_4a_desBuffer (Internal Data Memory)	0x02030000 (VXI Dual-Port RAM)	0xZZZZ 0002
5 **Set Point**	**5**	0x03000010	0x00000080	0x0000 ----	0x00500000+(Pulse ID)×offset (Async. SRAM)	0x03000014 (32k Set-Point FIFO)	0x00000000

Pulse ID=0,1,2,3,4,5,6,7 offset=0x00020000